Alexandrov RESEARCH INSTITUTE OF TECHNOLOGY
N I T I

Phase diagrams for multicomponent systems containing corium and products of its interaction with NPP materials
(CORPHAD)
Phase 2

PROGRESS REPORT

01/07/03 – 30/06/04

INVESTIGATION OF BINARY OXIDIC SYSTEMS:
SYSTEM UO_2-FeO

Project title	Phase diagrams for multicomponent systems containing corium and products of its interaction with NPP materials (CORPHAD, #1950.2)
Customer	ISTC
File specification	CORPHAD/RCP-0401
Place of project implementation	FGUP Alexandrov Research Institute of Technology (NITI) of the Russian Federal Agency for Atomic Energy Russia 188540, Sosnovy Bor of Leningrad Oblast, NITI

Project manager	Name	Yu. N. Aniskievich
	Signature	
	Date	October, 2004

Authors

Professor	V.B. Khabensky
Doctor	S.V. Bechta
Doctor	V.S. Granovsky
Academician	V.V. Gusarov
	S.A. Vitol
	E.V. Krushinov
Professor	Yu.B. Petrov
Doctor	S.Ju. Kotova
Doctor	A. A. Sulatskey
Doctor	I.V. Kulagin
Doctor	D.B. Lopukh
Doctor	A.Yu. Pechenkov
Doctor	L.P. Mezentseva
Doctor	A.V. Merzlyakov
	V.G. Blizniuk
	V.R. Bulighin
	E.M. Beliaeva
	E.K. Kaliago
	N.E. Kamensky
	A.V. Lisenko
	A.P. Martinov
	V.V. Martinov
	E.V. Shevchenko
	A.A. Chertkov
	V.I. Almjashev
	S.K. Kuchaeva
	N.A. Lomanova
	V.F. Popova

CONTENTS

Introduction

Knowledge about the phase diagram of corium is an indispensable condition for the correct modeling of molten pool structure and behavior under severe NPP accidents involving the core meltdown; thermal and physico-chemical phenomena taking place during the interaction of oxidic and metallic melts; and the interaction between corium and structures containing the molten pool. For the phase diagram construction it is necessary to know the phases existing in equilibrium within the system under any temperature and concentration of elements. The essential data: liquidus and solidus temperatures, the position of invariant points, compositions of phases in equilibrium, etc. are determined experimentally. This is the main method of investigation, but many labor-intensive experiments are necessary to ensure the reliability of a developed phase diagram. High temperatures of the melt, its chemical activity and other difficulties of the experimental studies substantially restrict the amount and reliability of experimental data. For this reason the theoretical methods of phase diagram construction and their application to the severe accident modeling, numeric codes, [1] are being intensively developed nowadays, e.g. GEMENY [2], DIATRIS [3], Thermocalc [4], Mtdata [5] and code-oriented data bases [6], e.g. IVTANTERMO [7], TDBCR [8], NUCLEA [9], NIST [10] But this methodology should be supported by experimental studies – both for binary diagram database establishment and optimization, and for multi-component diagrams – in order to verify numeric codes.

The reported work has been carried out within the ISTC CORPHAD project, which is aimed at specifying phase diagrams of corium-based systems and products of its interaction with NPP materials. The UO_2-FeO system phase diagram has been experimentally studied within the work.

The available publications provide very limited data on this system. The forecast of phase diagrams for the generic systems is presented in [11] (Fig. 1, dotted lines). The numeric prediction of the UO_2-FeO phase diagram, performed using the model of [11], is shown as a solid line. Phase equilibria in this system have also been studied in the CIT project [2] (Corium Interaction and Thermochemistry). The project, in which many CORPHAD team members were involved, studied the predicted eutectics region in the concentration range from 70 to 90 mass.% FeO; the eutectics point was determined as corresponding to 88.6 mass.% FeO and 1340°C temperature. Fig. 2 presents the results of that study.

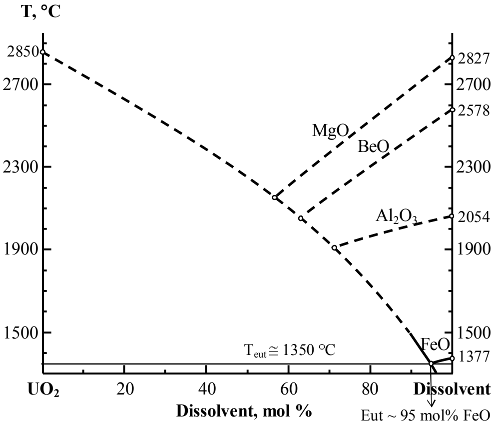

Dotted line from the data of [11]; solid line – calculations performed by the authors using the same model as in [11]

Fig. 1. UO_2 – FeO phase diagram prediction

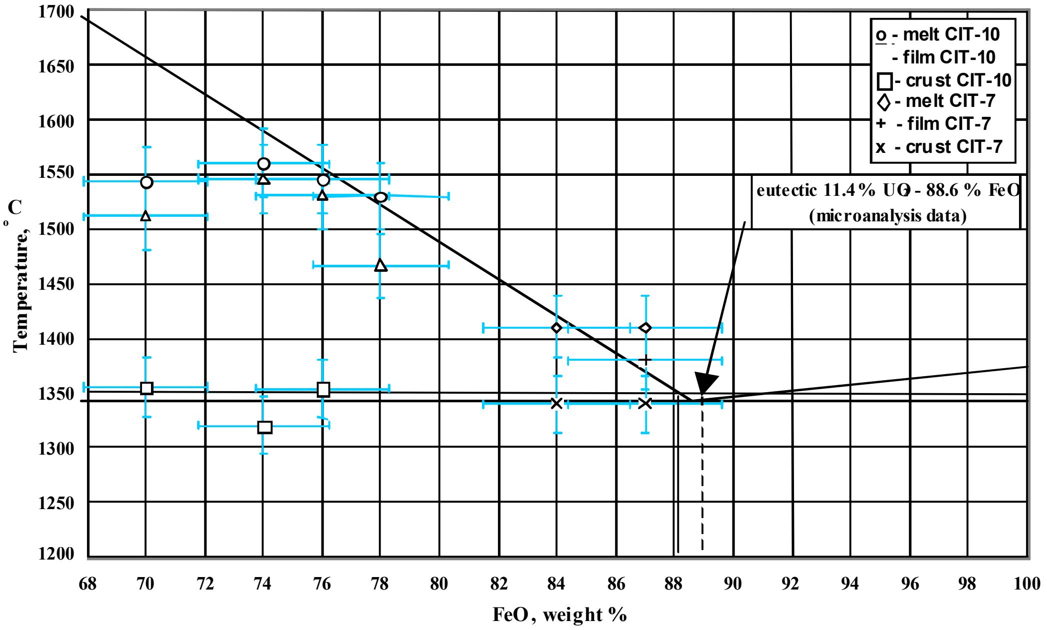

Fig. 2. Phase diagram of the UO_2 – FeO system in eutectics region in accordance with [12]

It is appropriate to mention studies of phase equilibria in the U-Fe-O system using the method of thermal balance followed by the isobaric ternary diagrams construction (N.M. Voronov et. al.) [13], but these investigations were made for high partial oxygen pressures in the system, 0.21 - 0.0058 atm., which corresponds to the quasi-binary diagrams of U3O8-Fe_2O_3 and UO_2-Fe_3O_4. In order to maintain the required stoichiometry a method based on the introduction of a stoichiometric getter, metallic iron, was developed and tested in our experiments [12].

The following objectives were set for the reported work:

- to determine liquidus and solidus temperatures in the wide range of the UO_2-FeO compositions in the inert atmosphere;
- to specify eutectics composition and temperature;
- to determine the final solubility of FeO in UO_2.

1. Methodologies and experimental facilities

At present there is no universally accepted method of phase diagram studies, which would provide reliable and accurate data on phase transformation temperatures, including solidus and liquidus temperatures, in the systems having a fixed composition and wide variations of atmosphere. Therefore, the continuous improvement of methods for the phase diagram studies was combined with the application of complementary methodologies, which increased the reliability of resulting data.

1.1 Visual polythermal analysis in a cold crucible

One of the classical methods of thermal analysis is the visual polythermal analysis (VPA) [13]. Its procedure includes the slow cooling of a crucible with melt in the furnace until first crystals appear on the molten pool surface. At this stage the surface temperature is registered; due to the slow cooling rate (1-2°C/min) and in absence of subcooling it is close to liquidus temperature. In accordance with [13] the error of this method does not exceed 10°C.

In most cases the application of this and other classical methods for the studies of corium-based systems is limited due to the high chemical activity of the melt. It interacts with crucible materials, which results in the melt pollution and, very often, in the failure to take measurements because of the crucible destruction. For this reason we have put forward a new VPA method applicable for the conditions of induction melting in a cold crucible (VPA IMCC), which lately has undergone a substantial adjustment for corium studies. Practically, it is the only method, which can be applied for studying high-temperature melts containing iron oxides.

The main IMCC peculiarity influencing the analysis accuracy and the character of melt crystallization is the thermal inhomogeneity of the pool contained within the water-cooled walls of the cold crucible. During the melt cooling its crystallization takes place both on the pool surface (like during VPA in the refractory or hot crucible) and on the interface of melt – bottom/side crusts produced on the cold crucible walls. This may result in the depletion of the refractory component in the melt; and the phase diagram point corresponding to the initial melt composition is located in the primary crystallization field of the refractory component. By the time, when first crystals appear on the molten pool surface its composition may not correspond to the initial melt composition. In the IMCC case the melt composition at the stage of crystal appearance is determined from the sample taken from the melt surface and subjected to the posttest physico-chemical analysis.

The originally-developed version of the VPA IMCC included the following stages:

1. The superheated molten pool was produced from the charge having a specified composition. The thickness of bottom crust was measured.
2. Power deposition in the melt was slowly decreased by stepping down the inductor voltage. The appearance of first crystals on the pool surface was registered. The first crystals on the melt surface were included into a viscous film having a darker coloring as compared to the initial melt.
3. The melt sample was taken as soon as the film appeared.
4. Frame-by-frame video-sequence was examined after the test, and the minimum temperature of the melt co-existing with film was determined.
5. Posttest physico-chemical analysis of the melt sample and identification of its composition were made.

This methodology has been checked using well-known phase diagrams, in particular ZrO_2-Nb_2O_5. Along with that, the measurements comparing the VPA IMCC data with DTA and DSC (differential scanning calorimetry) have been repeatedly performed. The resulting experimental data enabled to evaluate the liquidus temperature measurement error. It is the same as the pyrometer error in the composition range close to the eutectic. For refractory compositions with high fusion range the error is 50-75 °C. The above-described method was used in the studies carried out within the CIT and ENTHALPY projects [12,15-18]. The molten pool surface behavior was recorded on video (Fig. 1.1), and video-recorder was combined with pyrometer (3), which added the 50 Hz- frequency temperature measurements and position of the sighting spot to each still of the video sequence (Fig. 1.2) carried out using camera (3) and video recorder (6) (Fig. 1.1). Temperature on the molten pool surface was measured by the spectral ratio pyrometer RAYTEK MR1-SC. The camera monitored the region limited by the pyrometer shaft diameter, i.e. 22 mm. The pyrometer sighting spot is about 6 mm. The internal diameter of the cold crucible is 38 mm. The region not included into the recording is an 8-mm wide ring along the crucible wall.

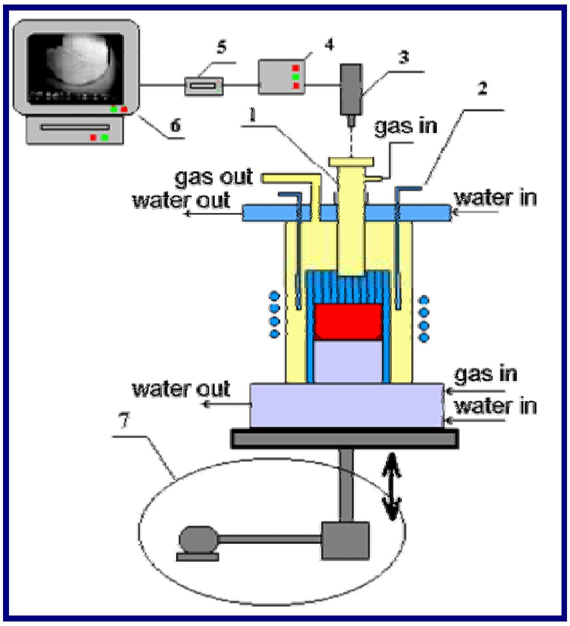

1-pyrometer shaft, 2- movable water-cooled electromagnetic screen, 3- pyrometer combined with video camera, 4-MDAS, 5- device for inserting measurement results into video-frames, 6- monitor/video recorder, 7- drive for vertical crucible movement

Fig. 1.1. Combined pyrometry – video recording system

It should be noted that the posttest analysis of melt composition, for which liquidus temperature was measured, complicates the methodology and delays the availability of results. In order to exclude changes in the melt composition at the VPA IMCC and, respectively, to reduce the complexity of posttest analysis, the method was improved by creating conditions for local cooling of the melt surface, the bulk of which was superheated. It was achieved (Fig. 1.1) by using the water-cooled electromagnetic screen, which was moved along the vertical crucible axis. When positioned against the thin surface layer of the superheated pool it provided the local temperature reduction and did not cause melt composition changes.

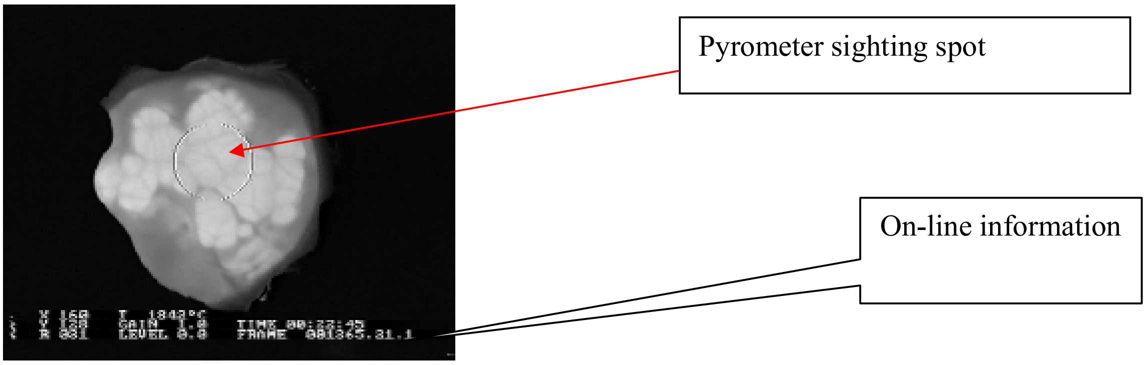

The melt surface temperature measured in the pyrometer sighting spot (white circle) and the time of the experiment are given in bottom lines

Fig. 1.2. A still of the molten pool surface

Fig. 1.3. gives an example of an experimental thermogram combined with the image of molten pool surface.

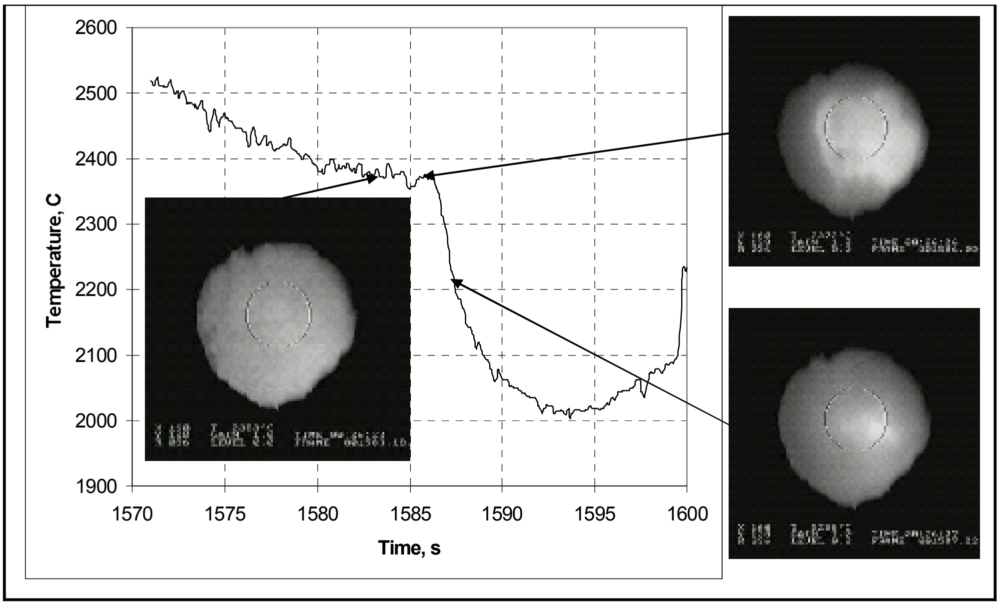

Fig. 1.3. A thermogram combined with images of the melt surface

At present the refined VPA IMCC methodology includes the following stages:

1. The superheated molten pool is produced from the charge having a specified composition. The thickness of bottom crust is measured.
2. A melt sample is taken.
3. The surface of superheated molten pool undergoes local cooling performed by moving the electromagnetic screen; the temperature and pool surface behavior are recorded.
4. The video is analyzed in a frame-by-frame way, the minimum melt temperature is determined.
5. Chemical posttest analysis of the melt sample and identification of its composition are performed (if necessary).

Let us consider the main sources of errors typical of the VPA IMCC methodology:

- Error in temperature and melt composition measurements. The relative error of pyrometric measurements integrating the error of a corresponding channel in the modular data acquisition system (MDAS) is 1%. Section 2.4 explains the error in determining composition by different methods of posttest analysis.

- Error caused by the melt subcooling. It has been confirmed by publications that in the non-equilibrium conditions the melt crystallization starts only after its subcooling to a certain degree. The degree of subcooling ΔT is a melt composition-specific, and in accordance with [20] it does not exceed 20-50 K. The direct measurement of ΔT of high-temperature oxidic melts under the IMCC conditions is not possible. The ΔT of melts can be derived from crystallization experiments using other methods. E.g., the direct ΔT measurements were conducted during the examination of the temperature axial gradient and subcooling on the crystallization front, when sapphire crystals were produced by the Stepanov method [19]. I was demonstrated that during the drawing of aluminium oxide crystals through the draw plate at a linear speed of 3-5 mm/min, subcooling ΔT of the melt on the meniscus was 30-45°C.

- Error caused by the temperature gradient and free convection of the molten pool in the IMCC conditions, which can be as high as 50°C [20].

Testing of the described methodology in the experiments with melts having well-known phase diagrams (Table 1.1), and the comparison of the VPA IMCC data with the results of DTA an DSC, in which the high-temperature microscope and Galakhov microfurnace were used, have shown that the total VPA IMCC error in determining liquidus temperature is equal to the temperature measurements error of the eutectics region compositions (or of pure oxides). In case of compositions having a wide fusibility range (over 200°C), and in their high-temperature region in particular, the error can be sufficiently higher, but, as a rule, it does not exceed 50-75°C.

Table 1.1. Comparison of melting temperatures (1), eutectics temperatures (2,3) and liquidus temperatures (4,5) determined by VPA IMCC and published data

No	Composition, mass %	VPA IMCC data, °C	Published data, °C	Source
1	100% Al_2O_3	2053	(2047-2054)±7	Samsonov, 1978
2	12% ZrO_2 88% Nb_2O_3	1411	1430	Toropov et al., 1969
3	19% ZrO_2 81% Fe_3O_4	1515	1520	Fischer and Hoffmann, 1957
4	21% ZrO_2 79% FeO	1611	1620	Fischer and Hoffmann, 1957
5	36.3% ZrO_2 73.7% FeO	1825	1835	Fischer and Hoffmann, 1957

A special methodology was used for determining the eutectics composition. According to it the melt was crystallized in the close-to-equilibrium conditions, which were achieved by slow (5-10 mm/h) uninterrupted driving of crucible versus inductor using drive (7) (Fig. 1.1). The posttest physicochemical analysis of samples from the last-to-crystallize ingot region enables to determine the eutectics composition with the 1-2 mass% error. The eutectics temperature (equal to solidus in case of simple eutectics systems) is determined by the VPA IMCC during the melting of corium having eutectics composition and later checked by other methods of thermal analysis.

The posttest analysis of ingots, produced by the equilibrium crystallization method described above, also enables a qualitative determination of the miscibility gap presence/absence in the system using the data on the ingot microstructure [21].

1.2 Galakhov method

Liquidus temperature has also been determined by the visual polythermal analysis in the Galakhov microfurnace [22].

Fig. 1.4 presents the microfurnace schematics. The microfurnace consists of a water-cooled metallic bottom, it is equipped by pipes for the evacuation of air and inert gas supply. The electrode holders are inserted into the furnace through the bottom. They are screened from it by mica plates, and the sealing liquid insulates them from the environment.

The spiral-shaped tungsten heater is incorporated into the electrode holders. The furnace experimental section is a 20-22 mm-high and 5.5-6 mm-wide cylinder (the zone of isothermal heating inside the heater). To reduce heat dissipation and achieve close-to-isothermal conditions the heater is surrounded by a molybdenum screen fastened to one of the supports.

A special device is used for putting a specimen into the microfurnace. The tested specimen is designed to have about 2 mm in diameter. It is inserted into the "eye" of a molybdenum or iridium 0.1-0.3 mm-thick wire-holder. The specimen location in the center of the isothermal zone is ensured by the specified wire length.

The microfinance is also designed for the specimen quenching (from the isothermal zone it can be dropped into the water-cooled channel).

The microfurnace is insulated from the environment by the water-cooled bell-jar. When heating is conducted in the inert atmosphere (to build up positive pressure) a special ring is used to press the jar to the base. The jar top has a quartz viewing window. The specimen melting and other transformations are recorded by the video system.

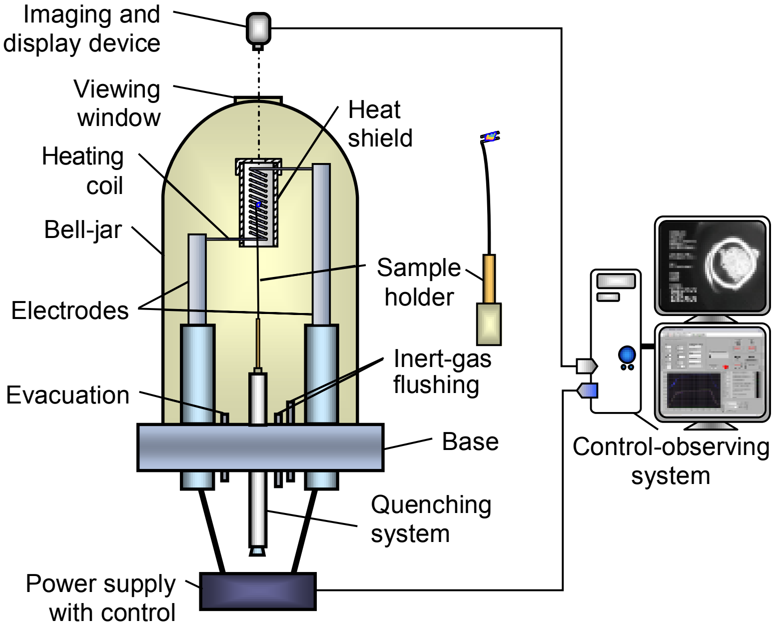

Fig. 1.4. Schematics of the Galakhov microfurnace

If the vacuum is not deep enough, the tungsten heater can get oxidized and tungsten oxide can be transferred to the specimen and cover it as a film, which may result in the melting temperature measurement errors. To avoid this the microfurnace is evacuated to $>10^{-5} – 10^{-6}$ atm. using a fore-evacuation and diffusion pumps. Following this the furnace is sparged with inert gas at least twice.

The temperatures, at which the observable changes in the specimen conditions take place, are determined from the curve of isothermal zone temperature vs. power supplied to the heater.

In order to construct the curve a series of reference meltings is performed, in which the substances having the established melting temperatures are used (Pt; Pd; Ag; Au; Cu; Al_2O_3 and others).

The heating is controlled automatically, and the heating and cooling curve is predetermined. The video recording is provided with temperature values recalculated from the power in the heater. The video signal is further processed on the computer. When the specimen spreads over the molybdenum (iridium) holder, the liquidus temperature is assumed to be reached.

There are at least four arguments for taking the specimen spreading in the Galakhov microfurnace for the liquidus temperature:

- heating produces a liquid phase very quickly (within 10 seconds). From this it can be inferred that we are fixing the point of low viscosity, because the high spreading rate is the indicator of such conditions;
- the specimen is prepared in such a way that its refractory phase would form a skeleton structure (rod quenching of a specimen under the IMCC conditions). In this way the prepared specimen starts spreading only after the skeleton destruction. It happens only in the case when the solid phase volume in the system does not exceed 5%.
- the specimen fast quenching is performed by its dropping from the heating zone. The microstructure of quenched specimens features the absence of unmolten regions, which testifies to the complete fusion of specimens;
- data of the visual polythermal analysis in the Galakhov microfurnace are confirmed by the data of differential thermal analysis, which is considered to be a classical method for phase diagram construction; and also by the data of other methods, the VPA IMCC in particular.

The range of experimental temperature measurements in the microfurnace is 900-2300°C. The experiments were conducted in the $10^{-5} – 10^{-6}$ atm. vacuum or in the inert atmosphere (argon, helium). The microfurnace is designed for experiments, when the inert gas pressure can be up to 1 atm. The maximum error of measurements in the mentioned temperature range is ±25°C.

1.3 Differential thermal analysis

French SETSYS Evolution-2400 analyzer was used for determining solidus and, if possible, liquidus temperatures by the DTA method.

SETSYS Evolution TAG-2400, (Fig. 1.5) operates in the temperature range from 196 °C to 2400 °C and used for the DSC, DTA, TG-DTA and TG-DSC measurements. Its precision is ±0.25 °C. The gas-proof experimental section can be evacuated and filled with air, argon, helium or carbonic acid. Such system provides the necessary information about oxidation-sensitive samples.

The SETSOFT software operates the device, provides data acquisition and processing.

The DTA was used only for determining solidus temperature, because liquidus measurements were not technically feasible due to the interaction between the resulting melt and crucible, which caused the sample composition changes. The specimens for studies were prepared from quenched melt samples or ingots. Solidus temperature was determined from the start of endothermic effect at specimen heating.

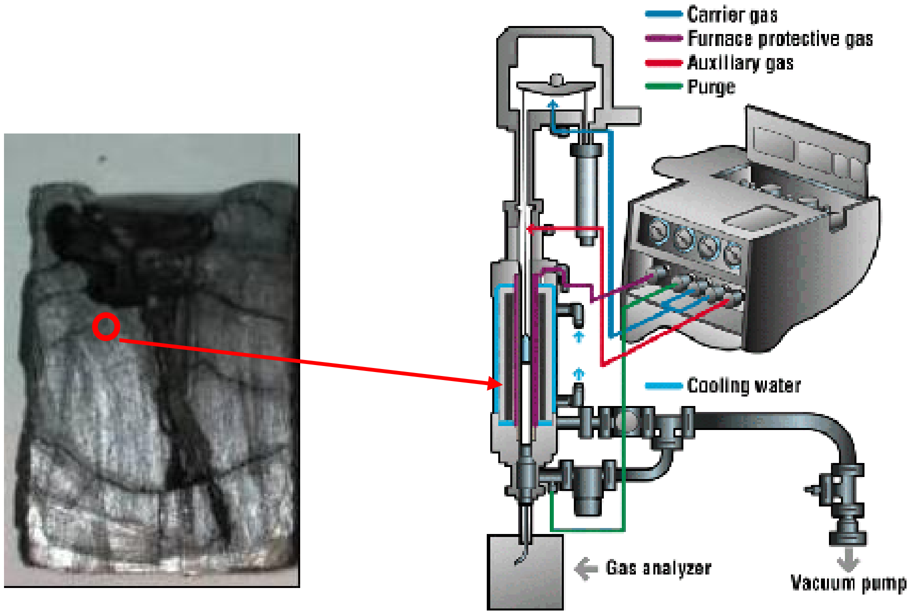

Fig. 1.5. System SETSYS Evolution-2400

2. IMCC tests of the CORD series

2.1. Charge analysis

Before the experiments the charge components, UO_2 and FeO (II) were analyzed for the content of basic substance and admixtures.

The content of metallic iron Fe^0 was determined by the copper-sulfate method.

The method is based on the displacement of copper by metallic iron, which takes place when powder is treated with copper sulfate [23]. Fe^{2+} ions equivalent to Fe_{met} are titrated with the dichromic acid calium solution in presence of redox indicator natrium difinylaminosupfonate.

The method enables to determine the concentration of metallic iron in powder, when iron concentration is below 0.5%.

The following reactions take place:

$$Fe+CuSO_4=FeSO_4+Cu\downarrow \tag{2.1}$$

$$6FeSO_4+K_2Cr_2O_7+7H_2SO_4=Cr_2(SO_4)_3+3Fe_2(SO_4)_3+K_2SO_4+7H_2O \tag{2.2}$$

The content of metallic iron (C, mass.%) is calculated from:

$$C_{Fe\ met.}=(100\times(a-b)\times T)/p\ , \tag{2.3}$$

where:

a – volume of 0.1n solution of dichromic acid calium, spent for titration, ml;

b – volume of 0.1n solution of dichromic acid calium, spent for the titration of the reference test solution, ml;

T – titre of 0.1n dichromic acid calium/potassium solution expressed as grams of metallic iron;

p – batch corresponding to the aliquot part of the solution taken for titration, g.

Fe(II) and Fe(III) content was determined by the photocolorimetry with orthophenanthroline.

The method is based on the reaction of orthophenanthroline (1.10-phenanthroline) and ions of ferrous iron, at which an orange-red complex is formed. The color intensity is in proportion to the iron concentration. Due to a high stability of the complex compound (formation constant is $9.8 \cdot 10^{21}$), the optical density does not depend on pH, if it is within the 2-9 range. The coloring develops fast at pH=3.0-3.5 in presence of excessive orthophenanthroline and it remains stable during several weeks. In more acidic solutions the coloring develops slower and it is not so intensive. A direct measurement of iron is possible when its mass concentration is between 0.5 - 2.0 mg/dm^3 [12]. The method enables to determine the content of ferrous iron and total iron in the solution separately. The content of ferric iron is calculated from the difference between the content of iron (II) and total iron [13]. The mass concentration of iron (X) in mg/dm^3 is calculated from:

$$X=(C\times 25)/V\,, \qquad (2.4)$$

where:
C – concentration of iron determined from the calibration graph, mg/dm^3;
V – volume of the aliquot iron sample taken for the determination, cm^3;
25 – volume, to which the sample was dissolved, cm^3.

Thermogravimetry was used for determining the O/U ratio in the uranium dioxide powder, it was 2.0.

The methodology is used for determining O/U in the UO_2 powder present in the charge composition, and in the molten UO^2 containing metallic admixtures in quantities below 0.5 mass.%, carbon and nitrogen – below 0.01 mass.%.

The determination method is based on the heating of powder containing $UO_{2\pm x}$ to U_3O_8 and calculation of O/U ratio from the mass change at heating [27,28] following the equation:

$$UO_x+(2.67-x)O \rightarrow UO_{2.67} \qquad (2.5)$$

It is calculated from:

$$O/U= (42.72A-280.75\Delta)/16.00A$$

where:
A – batch after the heating, g;
Δ – change of mass at the heating, g.

Table 2.1 presents the data on charge components.

Table 2.1. Charge composition

Components	Content of basic substance, %	Admixtures, mass %	Note
UO_2-powder with particle sizes <200μm	>99.0	Fe<0.03; As<0.0003; CuO<0.01; phosphates<0.002; chlorides<0.003.	Certificate data, thermogravimetry
FeO*	68.4	Fe_2O_3-29.6; Fe-0.5	Chemical analysis
FeO**	68.2	Fe_2O_3-30.0; Fe-0.7	Chemical analysis
FeO***	66.3	Fe_2O_3-32.4; Fe-0.9	Chemical analysis
Fe	>99.9	Si-0.0005; Mg-0.0001; Cu-0.0001; Ni-0.019; Pb-0.0001; Zn-0.00028	Certificate data

*- used in CORD-6,7,8
**- used in CORD-14, 22
***-used in CORD- 17-21, 23

2.2. *Specification of experiments*

All in all eleven experiments have been performed, their specification is given in Table 2.2.

Table 2.2. Specification of CORD 6-8, 14, 17-23 experiments

CORD	**Charge composition, mass%**				**Charge mass, g**	**Note**
	UO_2	**FeO**	**Fe**	**Fe, getter**		
6	39.28	54.38	5.35	0.99	173.1	T_{liq} measurements. Melt spillage
7	59.08	36.35	3.58	0.99	203.1	T_{liq} measurements. Melt spillage
8	11.16	80.02	7.83	0.99	153.4	Slow extraction of ingot Eutectics determination.
14	16.26	76.27	7.47	not introduced	156.3	Slow extraction of ingot Eutectics determination
17	39.50	53.88	5.63	0.99	374.7	T_{liq} measurements
18	59.30	35.94	3.77	0.99	419.9	T_{liq} measurements
19	49.25	45.31	4.44	0.99	395.9	T_{liq} measurements
20	16.17	75.01	7.83	0.99	334.5	Slow extraction of ingot Eutectics determination.
21	79.13	18.00	1.88	0.99	470.1	T_{liq} measurements
22	89.02	9.10	0.89	0.99	495.4	T_{liq} measurements
23	69.20	26.98	2.83	0.99	440.0	T_{liq} measurements

All experiments were conducted in the inert atmosphere (argon). In order to produce FeO metallic (carbonyl) iron was added into the furnace charge. A getter was added to the melt for FeO stoichiometry. Carbonyl iron was also used as a getter. Experiments CORD 6,7,8 were conducted in the "Rasplav-2" test facility, the rest – on "Rasplav-3".

2.3. *Experimental procedures*

Practically all procedures of T_{liq} measurement experiments were identical, they included the following stages:

- Charge materials were prepared and properly mixed in the argon atmosphere.
- The charge of specified composition was put into the furnace, which was sparged with argon.
- Molten pool was produced and superheated above the liquidus temperature.
- Molten pool depth and bottom crust thickness were measured.
- Melt sample was taken.
- Power deposition in the melt was reduced until films-crusts appeared (CORD 6,7) (the originally-developed version of the VPA IMCC method).
- The screen was lowered, and its position was fixed, when films-crusts appeared (CORD 8,14,17-23).
- The procedure of screen moving and fixing was repeated several times, the appearance of films-crusts was video-taped in order to determine T_{liq} (CORD 8,14,17-23).
- Heating was disconnected the surface was video-taped.
- Ingot was taken from the crucible and subjected to the posttest analysis.

During CORD 6, 7 on the "Rasplav-2" test facility the melt was spilled due to the intensive surface heating (the inductor current frequency was too high for the normal electric conductivity of the melt). For this reason later the "Rasplav-3" test facility was used and a lower inductor current frequency was applied. The experimental setup was modified in the following way:

- A new furnace having a larger-diameter crucible was designed and manufactured.
- A movable water-cooled electromagnetic screen was developed and manufactured for the implementation of improved methodology for T_{liq} measurements.

The experimental procedure for determining eutectics composition and temperature was different from the previous, it included the following stages:

- Charge materials were prepared and properly mixed in the argon atmosphere.
- The charge of specified composition was put into the furnace, which was sparged with argon.
- Molten pool was produced and superheated above the liquidus temperature.
- Molten pool depth and bottom crust thickness were measured.
- Crucible position was lowered versus the inductor until the generator reacted to this change of position (anode current dropped).
- Crucible driving mechanism was turned on (Section 7, Fig. 1.3).
- Ingot was slowly extracted from the inductor at 5-10 mm/h during 7-8 hours.
- Heating was disconnected; the surface was recorded on video.
- Ingot was taken from the crucible.
- Ingot was cut along the axis and a template for SEM/EDX analysis prepared.
- Last-to-crystallize liquid phase-eutectics region was identified by the SEM/EDX analysis, a sample was cut out from the region.

Three of the performed experiments have been aimed at determining the eutectics composition –CORD 8,14,20.

2.4. Posttest analysis

2.4.1. Chemical analysis

The chemical analysis of samples and ingots was performed in order to confirm the stoichiometric quality of initial oxides, as well as for determining the coordinate (composition) of the melt during the measurements of T_{liq} (eutectics).

The ingot and samples were analyzed for the content of Fe^0, Fe^{2+}, Fe^{3+}, U^{4+} and U^{6+}.

All preparations of samples for analysis were carried out in the argon atmosphere. At first the melt samples or ingot were crushed until the grain size was below 2 mm. After that an average sample was produced by quartering and subjected to further crushing, until the particle size was below 50 μm.

The content of Fe^0 was determined by the copper-sulfate method. Fe(II) and Fe(III) content was determined by the photocolorimetry with orthophenanthroline.

The methodology is used for determining the content of iron oxides in the samples of uranium-bearing corium without uranium separation [24]. The range of measured iron concentrations is 0.5-2.0 mg/dm^3. The total relative error of the method does not exceed ±3% on the condition that measured optical densities are within 0.2-0.6 nm.

The methodology of determining U^{+4}, U^{+6} using arsenazo III reagent is applied for identifying microquantities of uranium in corium samples, its sensitivity is 0.04 μg/ml [29, 30]. The method uses the property of quadrivalent uranium to form colored compounds with arsenazo III in 4 N HCl. Granulated zinc in presence of ascorbic acid is used for uranium reduction.

Quadrivalent uranium interacting with arsenazo III forms the green complex. If the reagent is in excess, violet coloring having different shades is observed. Spectrophotometry gives best results at 2-5-fold molar excess of reagent. The instantly appearing coloring stays for at least two hours.

The method enables to determine the content of quadrivalent uranium and total uranium in the solution separately. The hexavalent uranium is calculated from the difference between the content of total uranium) and uranium (IV).

Table 2.3 presents the results of determining Fe^0, Fe^{2+}, Fe^{3+}, U^{4+} and U^{6+}.

Table 2.3. Table 2.3. Chemical analysis of CORD-17-23 corium samples

CORD	Sample	Fe^0	Fe^{2+}	U^{4+}
		mass%		
17	Average sample of ingot	6.03	41.21	34.64
	Sample of melt #1	0.49	51.80	28.45
18	Average sample of ingot	2.45	27.77	53.39
	Sample of melt #1	0.42	37.14	45.27
	Sample of melt #2	0.30	39.03	43.50
	Rod sample of melt #1	0.55	37.34	45.00
19	Average sample of ingot	3.08	35.72	44.93
	Sample of melt #2	0.92	44.25	36.42
20	Average sample of ingot	7.95	52.61	14.63
21	Average sample of ingot	2.28	13.56	68.83
	Sample of melt #3	0.43	18.11	66.68
22	Average sample of ingot	4.05	4.81	78.9
	Sample of melt #1	0.23	8.71	77.98
23	Average sample of ingot	5.85	18.24	61.58
	Sample of melt #2	0.29	26.29	58.00

Notes to Table 2.3:

1. U^{6+} has not been detected in the samples.
2. Fe^{3+} has not been detected in the samples.

Table 2.4 gives errors of the completed chemical analyses.

Table 2.4. Errors of chemical analyses

Element	Error, % rel.	Method
U^{+6}	5	Photocolorimetry
U^{+4}	5	Photocolorimetry
Fe^0	10	Copper-sulfate
Fe^{+2}	5	Photocolorimetry
Fe^{+3}	5	Photocolorimetry

2.4.2. X-ray fluorescence (XRF)

The elemental composition of samples was determined by the X-ray fluorescence (XRF) method using SPARK-1M/IBM PC spectrometer [31] designed for the consecutive qualitative and quantitative determination of 66 chemical elements from Sc(21) to U(92) in a wide range of their concentrations in samples.

The specimens were prepared for investigations using the technique of compacted pellets. Two-layer pellets prepared from the mixture of uranium, zirconium and iron oxides molten in a small crucible (IMCC) were used as reference samples.

All specimens were prepared for analysis in the argon atmosphere. At first the samples were crushed down to the grain size below 2 mm. After that an average sample was produced by quartering and subjected to further crushing, until the particle size was below 50 µm.

Table 2.5 shows the XRF data of CORD 17-23 experiments.

Table 2.5. XRF data of CORD 17-23 corium samples

CORD	Sample	U	Fe	O*
		mass%		
17	Sample of melt #1	27.1	52.7	20.2
	Sample of melt #2	31.0	51.3	17.7
	Average sample of ingot	37.5	45.9	16.6
18	Sample of melt #3	49.8	35.1	15.1
	Sample of melt #4	45.6	39.1	15.3
	Rod sample of melt #1	48.7	35.7	15.6
	Rod sample of melt #2	48.1	36.4	15.5
	Average sample of ingot	56.0	31.0	13.0
19	Sample of melt #2	38.1	44.4	17.5
	Sample of melt #5	36.0	45.8	18.2
	Rod sample of melt #2	38.4	44.0	17.6
	Rod sample of melt #3	39.6	43.8	16.6
	Average sample of ingot	45.3	39.8	14.9
20	Average sample of ingot	15.4	66.3	18.3
21	Sample of melt #3	69.7	16.7	13.6
	Average sample of ingot	70.8	17.0	12.2
22	Sample of melt #1	80.1	8.0	11.9
	Average sample of ingot	77.7	8.7	13.6
23	Sample of melt #2	61.2	24.2	14.6
	Average sample of ingot	63.8	25.2	11.0

* oxygen was determined from the residue

2.4.3. Material balance of tests

For making the material balance of tests the initial charge components and molten products were weighed with 0.1 g accuracy.

Table 2.6 gives the mass balance of CORD 6-8, 14, 17-23 tests.

Table 2.6. CORD 6-8, 14, 17-23 material balance

Test	Introduced, g		**Collected, g**	
CORD 6	UO_2	68.0	Ingot	157.5
	FeO	94.1	From probe	5.9
	Fe	11.0	Ejections (spillages)	5.4
			Dry spillages	2.7
	Σ	173.1	Σ	171.5
	Imbalance	1.6		
CORD 7	UO_2	120.0	Ingot	66.2
	FeO	73.8	Ejections (spillages)	21.9
	Fe	9.3	Dry spillages	113.4
	Σ	203.1	Σ	201.5
	Imbalance	1.6		

CORD 8	UO_2	17.1	Ingot	139.2
	FeO	122.7	Probe	11.5
	Fe	13.6	Dry spillages	2.3
	Σ	153.4	Σ	153.0
	Imbalance	0.4		
CORD 14	UO_2	25.4	Ingot	135.5
	FeO	119.2	Probe	5.8
	Fe	11.7	Ejections (spillages)	11.5
			Dry spillages	2.5
	Σ	156.3	Σ	155.3
	Imbalance	1.0		
CORD 17	UO_2	148.0	Ingot	353.7
	FeO	201.9	Sample 1	1.8
	Fe	24.8	Sample 2	5.4
			Probe	8.3
			Dry spillages	3.7
	Σ	374.7	Σ	372.9
	Imbalance	1.8		
CORD 18	UO_2	249.0	Ingot	372.7
	FeO	150.9	Sample 3	4.2
	Fe	20.0	Sample 4	10.3
			From probe	9.2
			Dry spillages	6.2
			Rod sample 1	5.2
			Rod sample 2	10.4
	Σ	419.9	Σ	418.2
	Imbalance	1.7		
CORD 19	UO_2	195.0	Ingot	351.9
	FeO	179.4	Sample 2	4.3
	Fe	21.5	Sample 5	3.5
			From probe	16.5
			Dry spillages	6.9
			Rod sample 2	5.6
			Rod sample 3	5.3
	Σ	395.9	Σ	394.0
	Imbalance	1.9		
CORD 20	UO_2	54.1	Ingot	325.2
	FeO	250.9	Spillages	2.4
	Fe	29.5	From probe	1.4
			Dry spillages	4.6
	Σ	334.5	Σ	333.6
	Imbalance	0.9		
CORD 21	UO_2	372.0	Ingot	440.0
	FeO	84.6	Sample	7.6
	Fe	13.5	Probe	12.9
			Dry spillages	8.7
	Σ	470.1	Σ	469.2
	Imbalance	0.9		

CORD 22	UO_2	441.0	Ingot	471.3
	FeO	45.1	Sample	8.8
	Fe	9.3	From probe	7.5
			Dry spillages	7.6
	Σ	495.4	Σ	495.2
	Imbalance	0.2		
CORD 23	UO_2	304.5	Ingot	418.2
	FeO	118.7	Sample	11.1
	Fe	16.8	From probe	5.1
			Dry spillages	5.2
	Σ	440.0	Σ	439.6
	Imbalance	0.4		

Iron oxide compositions present in the charge are given in Table 2.1

Insignificant imbalance of experiments confirms the credibility of completed studies.

2.4.4. SEM/EDX analysis of ingots

The determination of ingot microstructure, elemental and phase composition was performed by the scanning electron microscopy (SEM) and energy-dispersion chemical analyses (EDX).

The examination of specimens by SEM was made using the scanning electron microscopes CamScan MV2300 and ABT-55. The elemental composition of chosen specimen sections was performed using the micro-probe devices ‘Oxford Link’.

The spectral characteristics of each specimen were determined. The characteristics were used for identifying the specimen integral composition and the composition of each separate phase. The quantitative analysis was performed by comparing spectrum intensities of the reference substance and studied specimen. The used extra-pure reference specimens of U, Zr, Cr, Fe, Si, Ca, Ni were taken from the microprobe reference kit.

The reliable identification limit of an element depends on its number in the Mendeleyev periodical table; it varies between 0.1 mass.% for light elements to 0.3 mass.% for heavy elements in case of the EDX-analyzer Oxford Link Pentafet, with which microscope CamScan MV2300 was equipped; and 0.5 mass.% for the EDX-analyzer Link using the ABT-55 microscope. The detection of elements present in smaller quantities is unreliable.

EDX-analyzer using microscope ABT-55 is not sensitive to light elements (to oxygen, in particular). For this reason oxygen was determined from the mass deficit; the oxygen determination error was ~5 mass.%.

The error of oxygen determination performed by the EDX-analyzer Oxford Link Pentafet is, as a rule, below 0.3 mass.%, but if iron-bearing systems are studied, the superposition of energy peaks takes place, which causes an additional error in determining both oxygen and iron.

The error in determining an average composition is the same as for separate phases. But:

- oxygen detection error considerably increases if a sample is very porous,

- the more inhomogeneous a sample is the less representative will be the average composition determined from a small area of a sample by, e.g., XRF (its normal scanning field is between 20x20 μm to 2x2 mm).

CORD 6 ingot studies

CORD 6 specimen taken from the ingot top was subjected to analysis. Fig. 2.1 shows the section picture with a specimen prepared for microanalysis. Fig. 2.2 shows the analysis results. The studied specimen surface is a part of the radial section including: a part near the cold crucible wall (Segment 1-1), a part having dendrite crystallization (Segment 1-2) and a part, where a typical eutectics crystallization pattern is observed (Segment 1-3).

First segment has the highest concentration of uranium oxide, it contains 90 mass.% UO_2 (area SQ1). The UO_2-based phase practically does not contain FeO (point P1).

In the second segment uranium oxide is depleted, it contains 22.4 mass.% UO_2 and 77.6 mass.% FeO (area SQ2). In accordance with EDX analysis the solubility of iron oxide in uranium dioxide is 1.2 mass.% (point P2). It is a dendrite-type phase. The typical size of its dendrites does not exceed 20 μm. The region between dendrites has a eutectics pattern of crystallization.

The concentration of uranium oxide in the third segment located closer to the ingot center is 14.7-15.1 mass.% (area SQ3), which is close to the predicted eutectics composition in this system. It should be noted that droplets of pure iron were found in this region (point P4), which testifies to the maintained stoichiometry of iron oxide as FeO (point P3).

Therefore, it can be asserted that during the test a fast precipitation of refractory component took place near the cold crucible walls and a strong shift of the initial composition towards the eutectics in the resulting melt (closer to the ingot center).

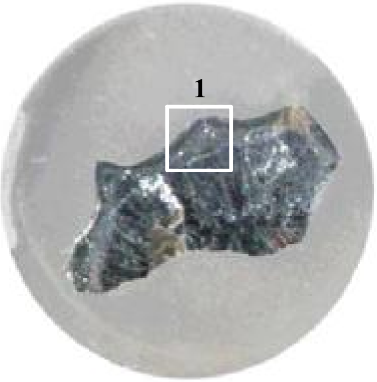

Fig. 2.1. Section containing a part of CORD 6 ingot. The SEM/EDX region is marked

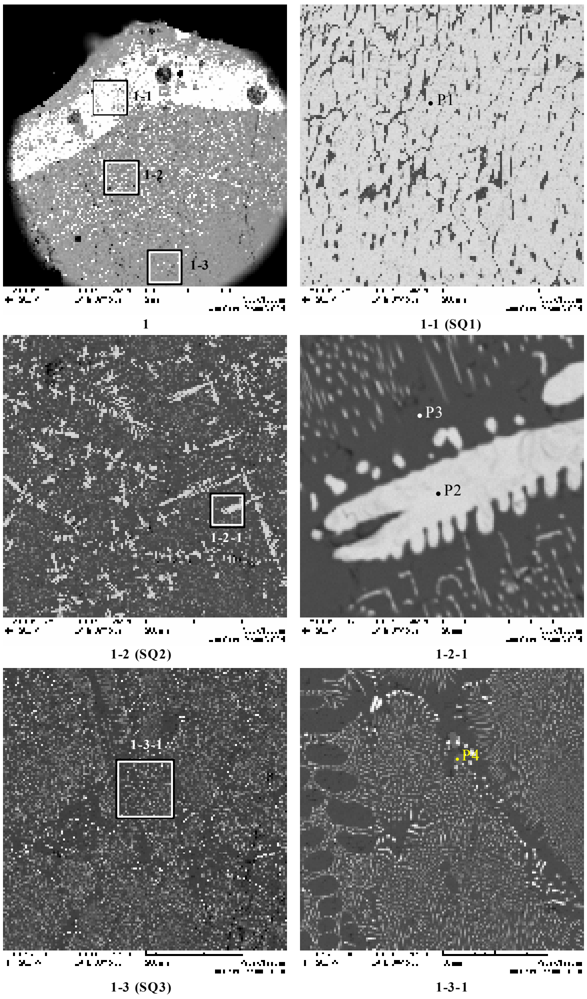

1 1-1 (SQ1)

1-2 (SQ2) 1-2-1

1-3 (SQ3) 1-3-1

No.		UO_2	FeO
SQ1	mass%	90.0	10.0
	mole%	70.5	29.5
SQ2	mass%	22.4	77.6
	mole%	7.1	92.9
SQ3	mass%	14.7	85.3
	mole%	4.4	95.6
P1		100 % UO_2	
P2	mass%	98.8	1.2
	mole%	95.5	4.5
P3		100 % FeO	
P4		100 % Fe	

Fig. 2.2. Microphotograph of Segment 1 from the CORD 6 specimen and EDX data

CORD 8 ingot studies

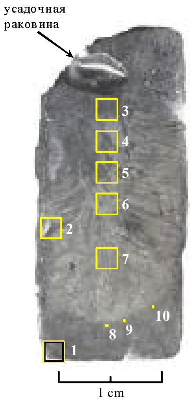

Fig. 2.3. Cross section of CORD 8 ingot, the studied segments are marked

Fig. 2.3 shows the studied segments of examined axial section. The results of CORD 8 ingot studies are presented in Figs. 2.4-2.9. The microphotograph of periphery ingot regions (segments 1, 2) demonstrates the layered structure of crystallization. The image of ingot bottom (Segment 1, Fig. 2.4) is typical for crystallization of system with miscibility gap – alternative layers of Fe (point P2) – FeO (point P3). It means that the excess of carbonyl iron added to the system as a getter crystallized in layers on the molten pool bottom. It also necessary to note that the UO_2-based phase crystallizes between Fe-FeO layers. In accordance with EDX the solubility of iron oxide in the uranium oxide is ~13.8 mass.% (Fig. 2.4, point P1), but this information can be considered only as qualitative due to extremely small dimensions of the phase (~1 μm). In order to determine the iron oxide solubility limit more exactly, an attempt was made to find the grown UO_2 grains in the boundary layers of eutectics zone (Fig. 2.3, segments 8-10).

The ingot side (Region 2, Fig. 2.5) also has a layered structure, but its origin is different from the bottom region. In this case these are alternating layers of pure FeO and crystallized melt having the eutectics character of crystallization. The concentration of uranium oxide in the zone is ~19.6 mass.% (area SQ1).

Segments 3, 4, 5 and 6 located at an equal distance from each other were examined in the vertical direction from the shrink hole (Fig. 2.3). The concentration of uranium oxide in these segments was as follows: 12.0 mass.% (Fig. 2.6, area SQ1), 18.1 mass.% (Fig. 2.6, area SQ2), 16.3 mass.% (Fig. 2.7, area SQ1), 15.2 mass.% (Fig. 2.8, area SQ1) respectively. Fig. 2.10 shows the graphic comparison of EDX analysis data for these segments. The spectra have no qualitative differences, which testifies to the similarity of the compositions.

The content of uranium oxide in Segment 7 (Fig. 2.3), which is located closer to the specimen bottom, is 15.4 mass.% (Fig. 2.8, area SQ2).

The final solubility of iron oxide in the uranium oxide in regions 1-7 could not be determined due to very small sizes of UO_2-based phases (Fig. 2.3-2.8). In order to determine the content of FeO in UO_2 three regions were additionally chosen on the eutectics zone boundary, in which the size of UO_2-based phase is large enough for analysis (segments 8-10, Fig. 2.3, and phases P1, P2, P3 in Fig. 2.9). The content of iron oxide in them varies between 2.9 mass.% (point P2) and 4 mass.% (point P3). The size of these segments is about 5 μm, which is still insufficient for accurate analysis.

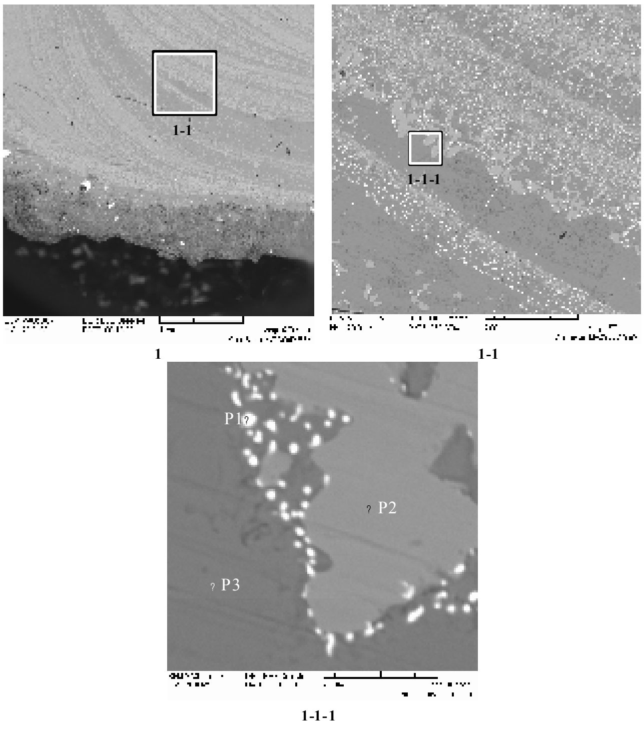

1

1-1

1-1-1

No.		UO_2	FeO
P1	mass%	86.2	13.8
	mole%	62.4	37.5
P2		100 % Fe	
P3		100 % FeO	

Fig. 2.4. Microphotographs of Segment 1. EDX analysis data

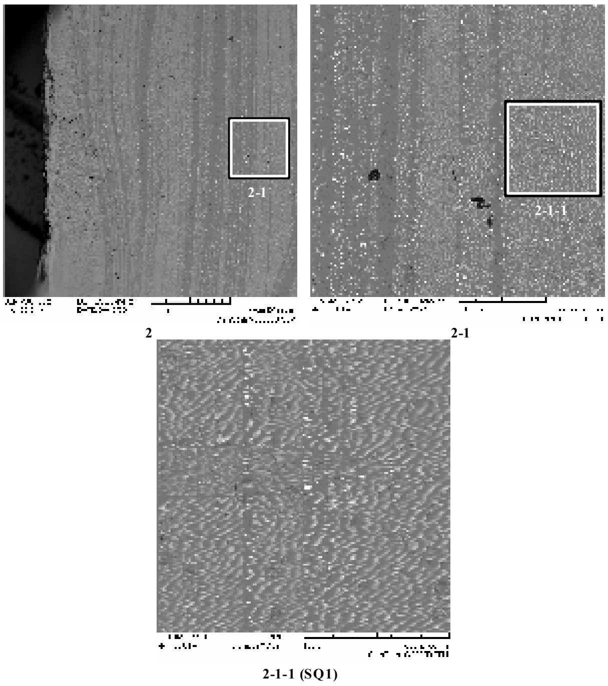

2 2-1

2-1-1 (SQ1)

No.		UO_2	FeO
SQ1	mass%	19.6	80.4
	mole%	6.1	93.9

Fig. 2.5. Microphotographs of Segment 2. EDX analysis data

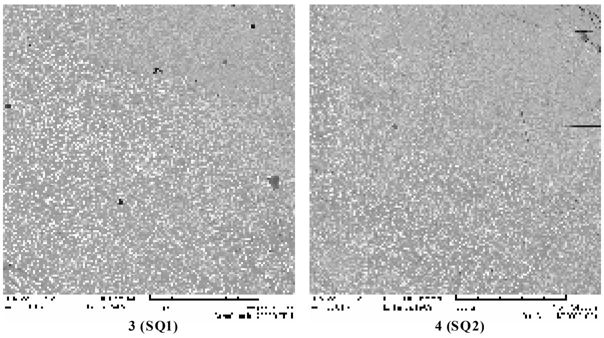

3 (SQ1) 4 (SQ2)

No.		UO_2	FeO
SQ1	mass%	12.0	88.0
	mole%	3.5	96.5
SQ2	mass%	18.1	81.9
	mole%	5.5	94.5

Fig. 2.6. Microphotographs of Segments 3 and 4. EDX analysis data

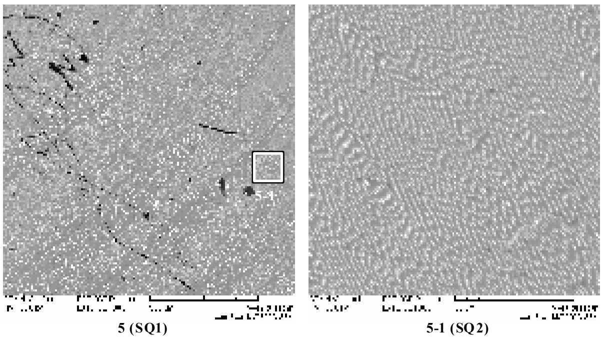

5 (SQ1) 5-1 (SQ2)

No.		UO_2	FeO
SQ1	mass%	16.3	83.7
	mole%	4.9	95.1
SQ2	mass%	16.6	83.4
	mole%	5.0	95.0

Fig. 2.7. Microphotographs of Segment 5. EDX analysis data

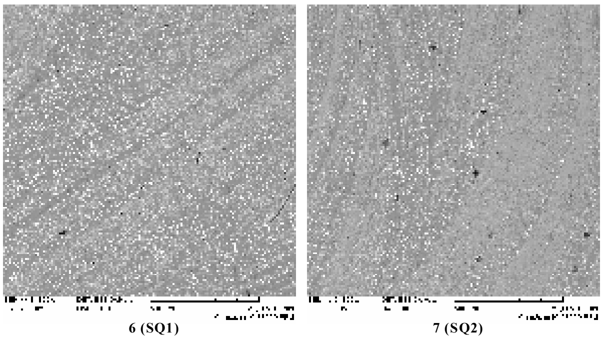

6 (SQ1)

7 (SQ2)

No.		UO_2	FeO
SQ1	mass%	15.2	84.8
	mole%	4.5	95.5
SQ2	mass%	15.4	84.6
	mole%	4.6	95.4

Fig. 2.8. Microphotographs of Segments 6 and 7. EDX analysis data

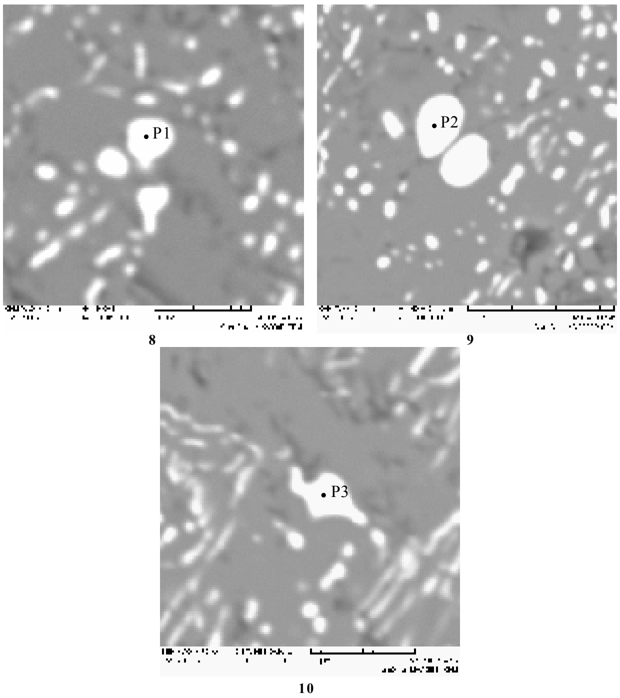

8

9

10

No.		UO_2	FeO
P1	mass%	96.4	3.6
	mole%	87.7	12.3
P2	mass%	97.1	2.9
	mole%	90.0	10.0
P3	mass%	96.0	4.0
	mole%	86.4	13.6

Fig. 2.9. Microphotographs of segments 8-10. EDX-analysis data

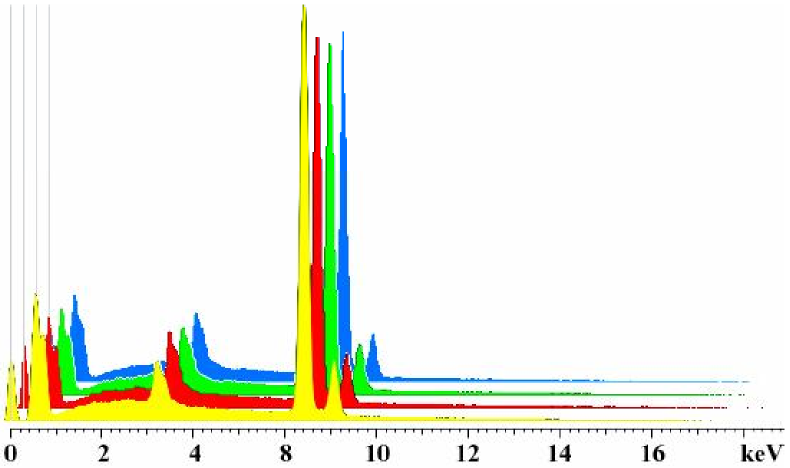

Fig. 2.10. Comparison of EDX-analysis data of segments 3, 4, 5 and 6

CORD 17 ingot studies

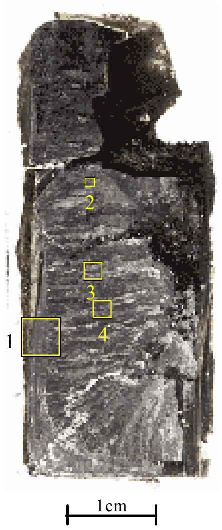

Fig. 2.11. Axial section of CORD 17 ingot with studied segments

The studied locations of the axial ingot half are presented in Fig. 2.11. The results of CORD 17 ingot studies are presented in Figs. 2.12-2.15.

The microphotograph of ingot periphery (Segment 1, Fig. 2.12) demonstrates the presence of crystallized metallic iron in large concentrations. At 3 mm depth the alternating Fe-FeO and FeO layers can be found, the latter contains precipitated UO_2-based inclusions.

The average composition of the central part has a considerable UO_2 depletion as compared to its mass in the original charge. Uranium does not exceed 23 mass. % UO_2 (Fig. 2.14 area SQ1, Fig. 2.15 area SQ1).

It can be derived from crystallization character that the central ingot part is a eutectics zone having the UO2-based dendrites. This dendrite-type crystallization phase occupies about 10-15 vol.% of the total area. The typical size of dendrites is about 200 μm, but the phase is not more than 30 μm in diameter. In accordance with EDX data the solubility of iron oxide in the uranium oxide is ~1-1.5 mass.% (Fig. 2.13 point P1, Fig. 2.15 point P1). Suchlike crystallization pattern is an evidence to the insufficiently quenching conditions for this system, and at crystallization UO_2 easily releases FeO into the ambient melt (Figs. 2.13 and 2.15), because of this the final solubility of FeO in UO_2 determined by EDX can be lower than actual.

EDX analysis of eutectics zone between dendrites gives the concentration of uranium oxide ~12.5 mass.% (Fig. 2.13 area SQ1).

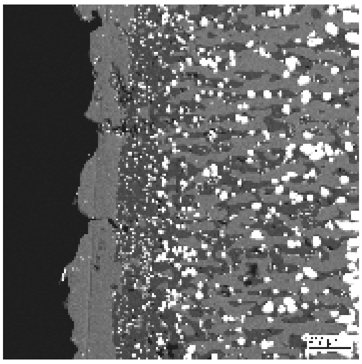

Fig. 2.12. Microphotograph of Segment 1

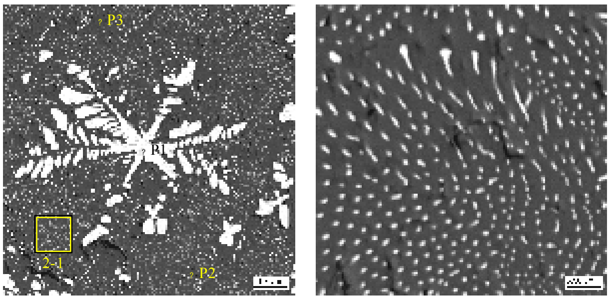

2 2-1 (SQ1)

No.		UO_2	FeO
SQ1	mass%	12.48	87.52
	mole%	3.65	96.35
P1	mass%	99.06	0.94
	mole%	96.55	3.45
P2	mass%	2.66	97.34
	mole%	0.72	99.28
P3		100 % FeO	

Fig. 2.13. Microphotograph of Segment 2. EDX-analysis data

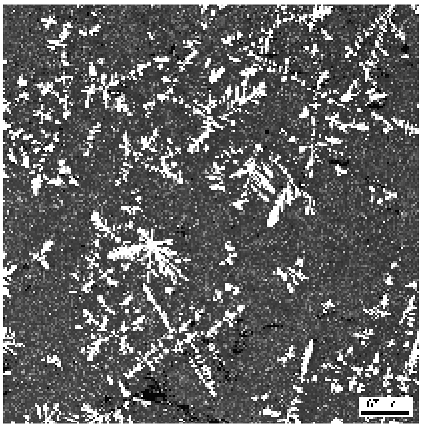

No.		UO_2	FeO
SQ1	mass%	22.6	77.4
	mole%	7.21	92.79

Fig. 2.14. Microphotograph of Segment 3 (SQ1). EDX-analysis data

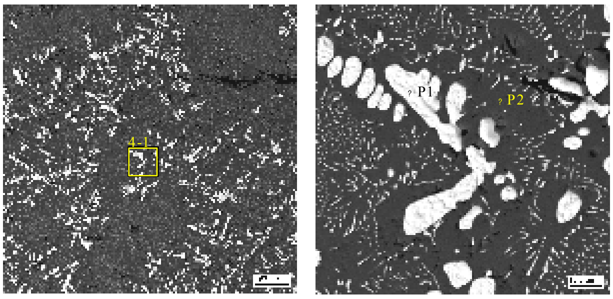

4 (SQ1) 4-1

No.		UO_2	FeO
SQ1	mass%	21.74	78.26
	mole%	6.88	93.12
P1	mass%	98.77	1.23
	mole%	95.54	4.46
P2		100 % FeO	

Fig. 2.15. Microphotograph of Segment 4. EDX-analysis data

CORD 18 ingot studies

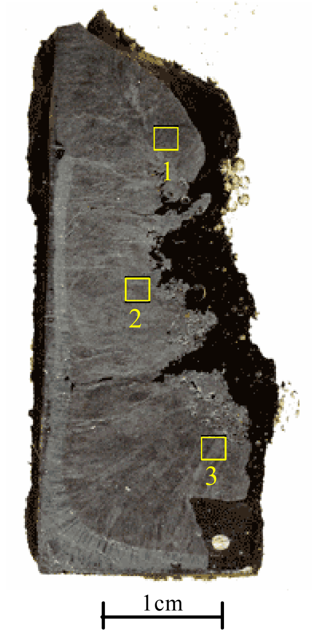

Fig. 2.16. CORD 18 template with studied segments

Fig. 2.16 shows the studied locations of the axial ingot section. The SEM/EDX data of CORD 18 ingot are presented in Fig. 2.17-2.19.

The crystallization character of the ingot periphery region is the same as CORD 17.

The average composition of the central ingot part has a considerable UO_2 depletion as compared to the original mass of UO_2 in the charge, its posttest concentration increases from the shrink region (Fig. 2.17 area SQ1 - ~35 mass.% UO_2) to the bottom (Fig. 2.19, Segment 3 area SQ1 - ~43 mass.% UO_2).

The crystallization pattern of the central ingot part is similar to CORD-17, but it has much lower eutectics, and UO_2-based dendrites take ~40-50 vol.%. The dendrites are longer than in the similar CORD 17 region, but the branch cross-section is the same, about 30 μm, and they are also bordered by the pure phase of FeO. In accordance with EDX the solubility of iron oxide in uranium oxide is ~1.5 mass.% (Fig. 2.18 point P1).

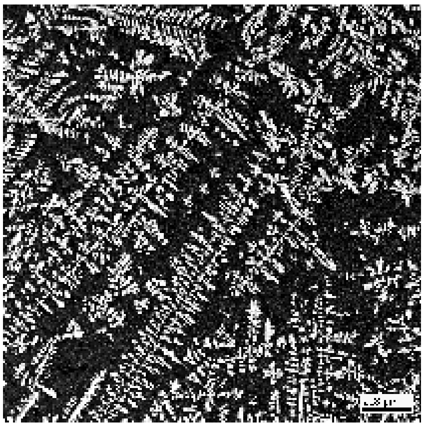

1(SQ1)

No.		UO_2	FeO
SQ1	mass%	35.4	64.6
	mole%	12.73	87.27

Fig. 2.17. Microphotograph of Segment 1. EDX-analysis data

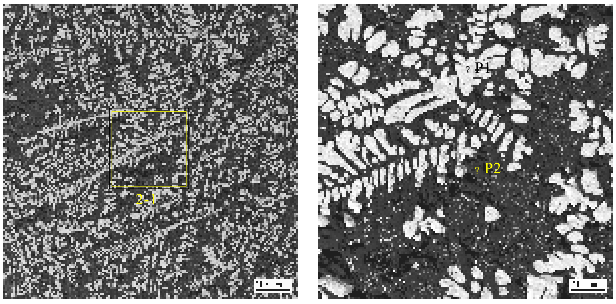

2 (SQ1) 2-1

No.		UO_2	FeO
SQ1	mass%	38.5	61.5
	mole%	14.28	85.72
P1	mass%	98.5	1.5
	mole%	94.59	5.41
P2		100 % FeO	

Fig. 2.18. Microphotograph of Segment 2. EDX-analysis data

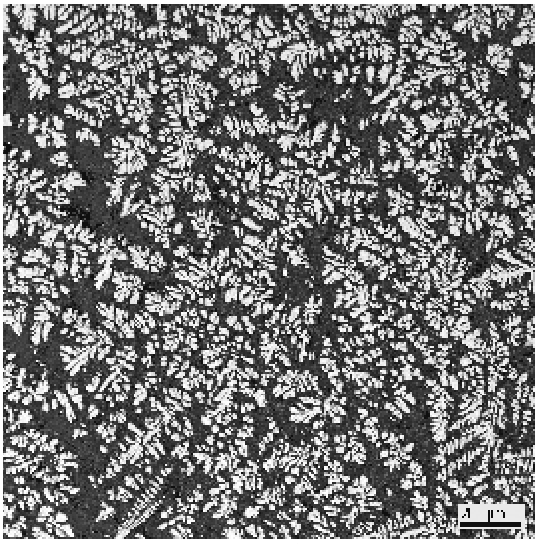

3(SQ1)

No.		UO_2	FeO
SQ1	mass%	42.74	57.26
	mole%	16.57	83.43

Fig. 2.19. Microphotograph of Segment 3. EDX-analysis data

CORD 19 ingot studies

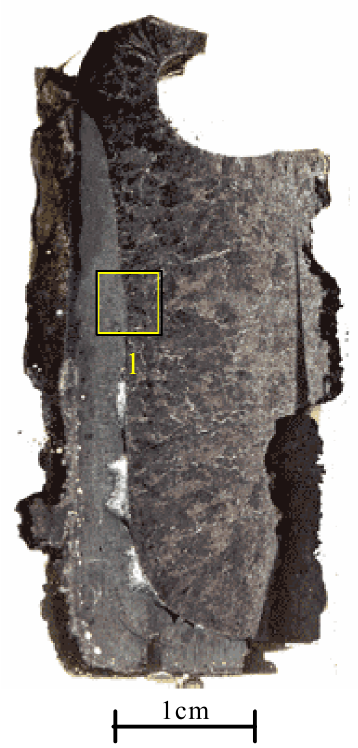

Fig. 2.20. CORD 19 template with studied segments

Fig. 2.20 shows studied segments of CORD-19 ingot axial section. The SEM/EDX data of CORD 19 ingot are presented in Fig. 2.21.

In accordance with CORD 19 experimental procedure the equilibrium crystallization layer was grown by the ingot extraction from the inductor at 8-10 mm/hr during two hours. This resulted in the formation of a nearly-mono-crystalline UO_2 layer with dissolved FeO in the periphery ingot region.

UO_2 in the central ingot part is depleted (in this case due to the formed layer of equilibrium crystallization) as compared to its mass in the original charge (Fig. 2.21 area SQ2 - ~19 mass.% UO_2).

In terms of crystallization pattern the central part is similar to CORD 17, but its eutectics zone is large, UO_2-based dendrites occupy ~5-10 vol.%. The dendrites are smaller than those in the similar region of CORD 17, the branch diameter is about 10 μm. It is expedient to determine the final solubility of iron oxide in the equilibrium crystallization zone, where FeO remains between UO_2 grains. In accordance with EDX the average composition in this zone (Fig. 2.21, area SQ1) corresponds to ~5 mass.% FeO. This value can be taken as the solubility limit in the region corresponding to the average composition of the crystallized central part of the ingot, i.e. ~19 mass.% UO_2 (Fig. 2.21 area SQ2).

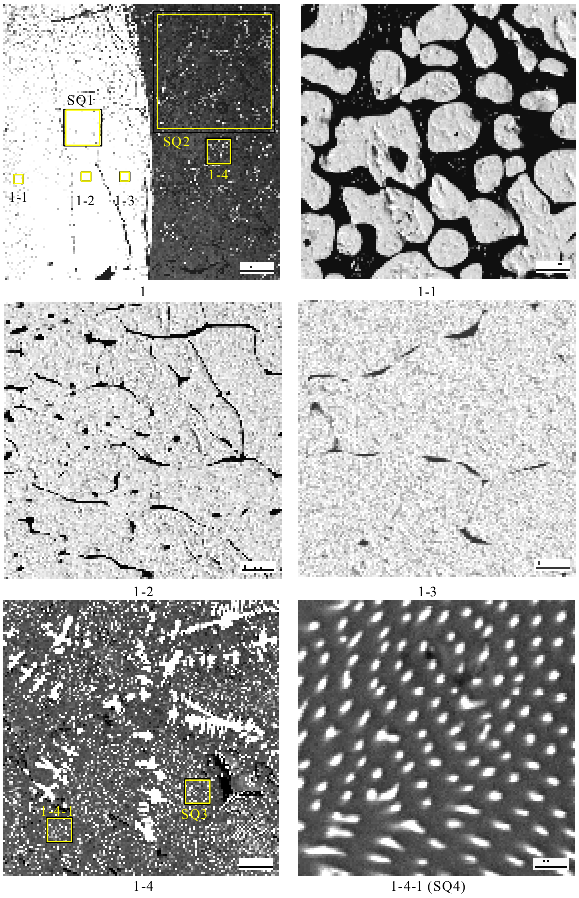

1 1-1 1-2 1-3 1-4 1-4-1 (SQ4)

No.		UO_2	FeO
SQ1	mass%	94.92	5.08
	mole%	83.26	16.74
SQ2	mass%	18.73	81.27
	mole%	5.78	94.22
SQ3	mass%	14.41	85.59
	mole%	4.29	95.71
SQ4	mass%	15.91	84.09
	mole%	4.79	95.21

Fig. 2.21. Microphotograph of Segment 1. EDX-analysis data

CORD 20 ingot studies

Fig. 2.22. CORD 20 template with studied segments

Fig. 2.22 shows the segments studied in the axial section of the CORD 20 ingot. The SEM/EDX data of the CORD 20 ingot are presented in Figs. 2.23-2.26.

The experiment was aimed at specifying the eutectics position. The initial charge composition was specified after the CORD 8 ingot analysis.

The SEM/EDX data of the ingot bottom shows the presence of UO_2-based refractory phase (Fig. 2.26 point P1), which coexists with the eutectics (Fig. 2.26, area SQ1).

The average composition of the eutectics zone near the shrink pore (crystallization region of the last, most fusible composition) corresponds to the UO_2 content 13.4-13.7 mass.% (Fig. 2.23, areas SQ1 and SQ2). This phase ratio corresponds to the eutectics composition of this system.

It is difficult to determine the final solubility of iron oxide in this test due to the small size of phases in the UO_2 zone, and easy migration of FeO from UO_2 in the subsolidus region of the diagram. In accordance with EDX the FeO solubility is about 1.2-2.8 mass.% (Fig. 2.24, point P1, Fig. 2.26, point P1), but more accurate data are provided by the analysis of the equilibrium crystallization zone, which was performed during the CORD 19 ingot studies

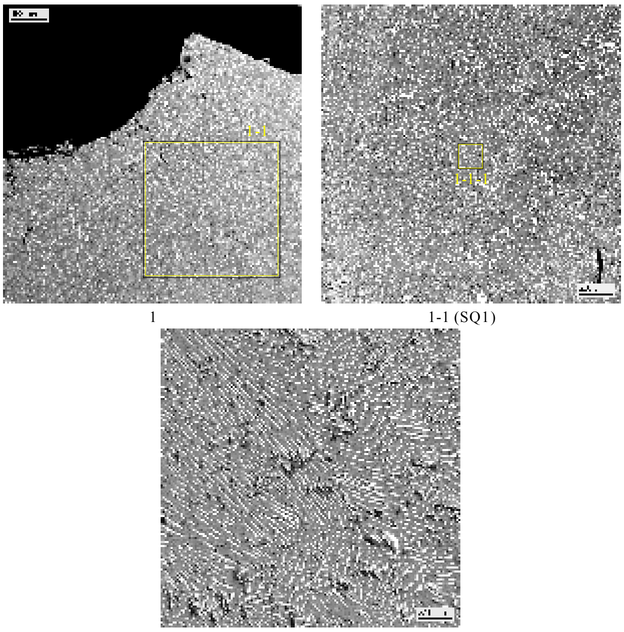

1

1-1 (SQ1)

1-1-1 (SQ2)

No.		UO_2	FeO
SQ1	mass%	13.41	86.59
	mole%	3.96	96.04
SQ2	mass%	13.72	86.28
	mole%	4.06	95.94

Fig. 2.23. Microphotographs of Segment 1. EDX-analysis data

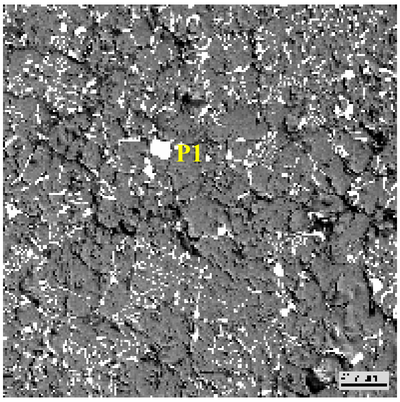

No.		UO_2	FeO
P1	mass%	97.25	2.75
	mole%	90.39	9.61

Fig. 2.24. Microphotograph of Segment 2. EDX-analysis data

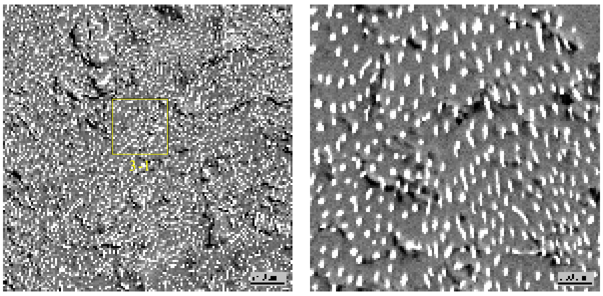

3 (SQ1) 3-1 (SQ2)

No.		UO_2	FeO
SQ1	mass%	14.34	85.66
	mole%	4.26	95.74
SQ2	mass%	13.26	86.74
	mole%	3.91	96.09

Fig. 2.25. Microphotographs of Segment 3. EDX-analysis data

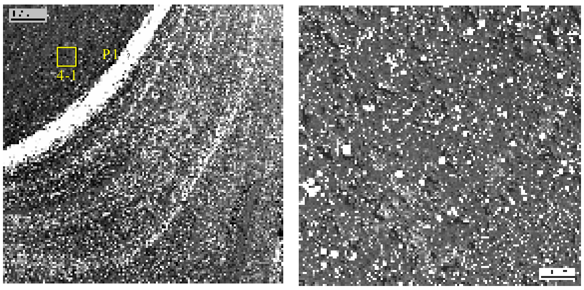

4 4-1 (SQ1)

No.		UO_2	FeO
SQ1	mass%	14.26	85.74
	mole%	4.24	95.76
P1	mass%	98.73	1.27
	mole%	95.39	4.61

Fig. 2.26. Microphotographs of Segment 4. EDX-analysis data

CORD 21 ingot studies

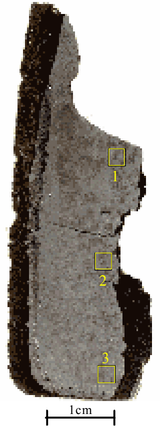

Fig. 2.27. CORD 21 template with studied segments

Fig. 2.27 shows the studied segments of CORD 21 axial section. The SEM/EDX data of CORD 21 ingot are presented in Figs. 2.28-2.30.

The crystallization pattern of its periphery region is similar to CORD 17 and CORD 18. Like in the whole experimental series, UO_2 is considerably depleted in the central ingot part as compared to the initial charge; and UO_2 concentration grows from the shrink region (Fig. 2.28 area SQ1 - ~58 mass.% UO_2) towards the center (Fig. 2.29 area SQ1 - ~68 mass.% UO_2). UO_2 concentration drops near the bottom (Fig. 2.30, area SQ1 - ~66 mass.% UO_2). The central ingot part has the dendrite crystallization character. The dendrites occupy ~90 % of the total area, they are long (~100 μm) the diameter of their branches is ~30 μm. FeO phase is concentrated around the dendrites, it is crossed with UO_2 threads in some locations (small crystallized eutectics zones). In accordance with EDX the solubility of iron oxide in uranium oxide is ~1.2-1.7 mass.% (Fig. 2.28, point P1; Fig. 2.30, point P1).

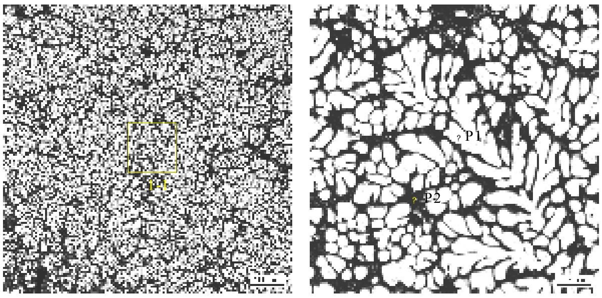

1 (SQ1) 1-1

No.		UO_2	FeO
SQ1	mass%	58.33	41.67
	mole%	27.14	72.86
P1	mass%	98.33	1.67
	mole%	94	6
P2	mass%	4.48	95.52
	mole%	1.23	98.77

Fig. 2.28. Microphotographs of Segment 1. EDX-analysis data

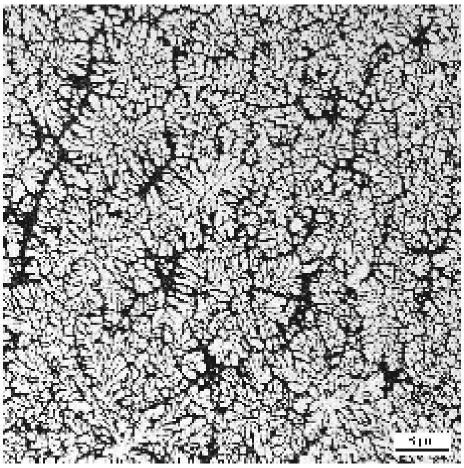

No.		UO_2	FeO
SQ1	mass%	67.73	32.27
	mole%	35.83	64.17

2(SQ1)

Fig. 2.29. Microphotograph of Segment 2. EDX-analysis data

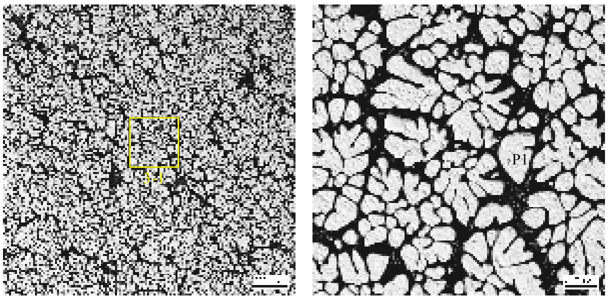

3 (SQ1) 3-1

No.		UO_2	FeO
SQ1	mass%	65.89	34.11
	mole%	33.95	66.05
P1	mass%	98.81	1.19
	mole%	95.67	4.33

Fig. 2.30. Microphotographs of Segment 3. EDX-analysis data

CORD 23 ingot studies

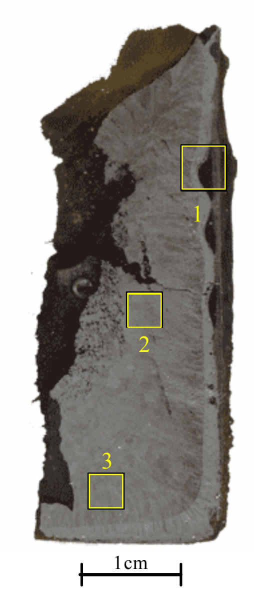

Fig. 2.31. CORD 23 template with studied segments

Fig. 2.31 shows the location of segments studied in the ingot axial section.

The SEM/EDX studies of CORD 23 ingot are presented in Fig. 2.32.

The crystallized pure iron is found on the ingot periphery, it is followed by the refractory component (Segment 1).

UO_2 is considerably depleted in the ingot central part as compared to its mass in the initial charge (segment 2, area SQ1 - ~49 mass.% UO_2).

The dendrite-type crystallization is observed in the central ingot part. The dendrites occupy about 80% of the total area, they are rather long (~250 μm), their diameter is ~30 μm. The dendrites are crystallized in the matrix having the eutectics crystallization character (similar to CORD 6, CORD 17, CORD 18 etc.). In accordance with EDX data the iron oxide solubility in iron oxide is ~1.4 mass.% (Fig. 2.32. point P1).

It should be noted that due to the non-equilibrium crystallization all studied ingots (except eutectics CORD 8 and CORD 20) have radial and axial inhomogeneity of composition, in which fusible components crystallize mostly in the ingot top and center. This complicates the analysis, the VPA studies of samples and phase diagram construction. The carbonyl iron added as a getter is also an additional complicating factor for the VPA and DTA analyses, but it guarantees stoichiometry of iron oxide in the form of wustite.

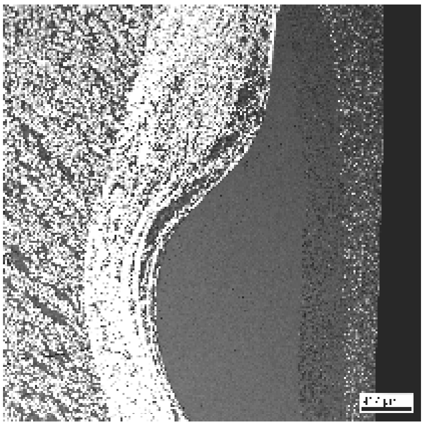

Segment 1

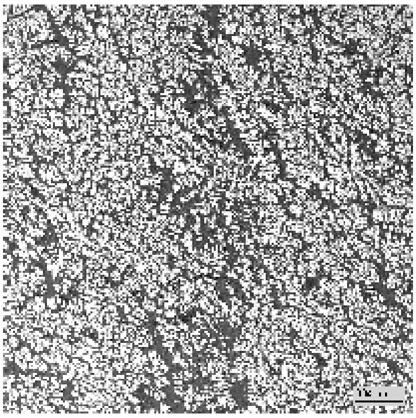

Segment 3

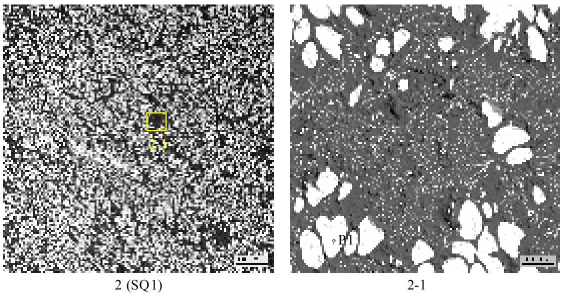

2 (SQ1)

2-1

Segment 2

No.		UO_2	FeO
SQ1	mass%	49.31	50.69
	mole%	20.56	79.44
P1	mass%	98.56	1.44
	mole%	94.79	5.21

Fig. 2.32. Microphotographs of segments 1,2,3. EDX-analysis data of segment 2

2.4.5. Overview of the VPA IMCC data

Fig. 2.33-2.37 and Table 2.7 present the overview of data produced during the UO_2-FeO studies by the VPA IMCC. The figures show fragments of thermograms with melt surface images at the time, when T_{liq} was measured. The CORD 6, 7 data have not been processed, because the experiments were terminated for technological reasons.

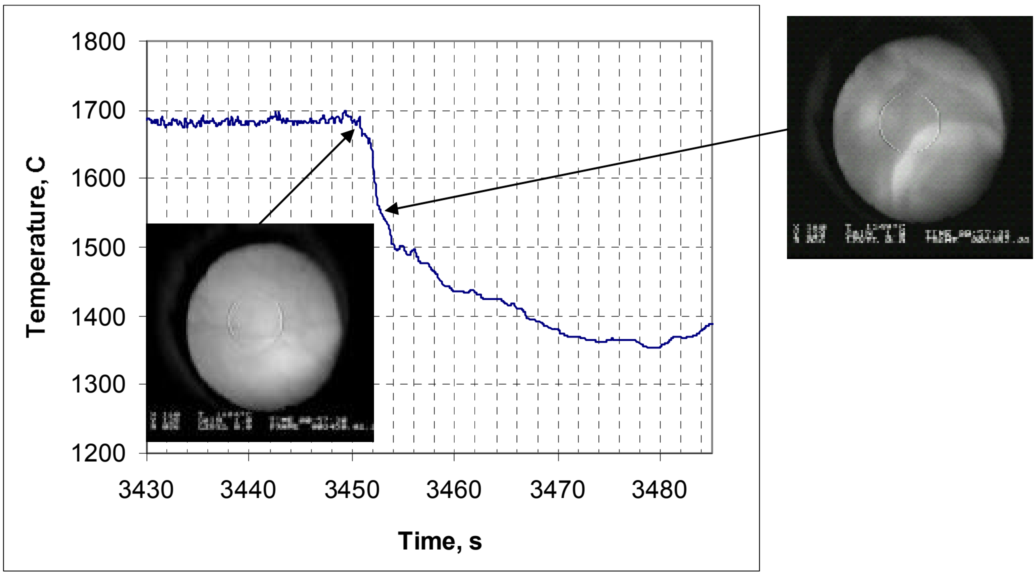

Fig. 2.33. Fragment of CORD 17 thermogram with melt surface images

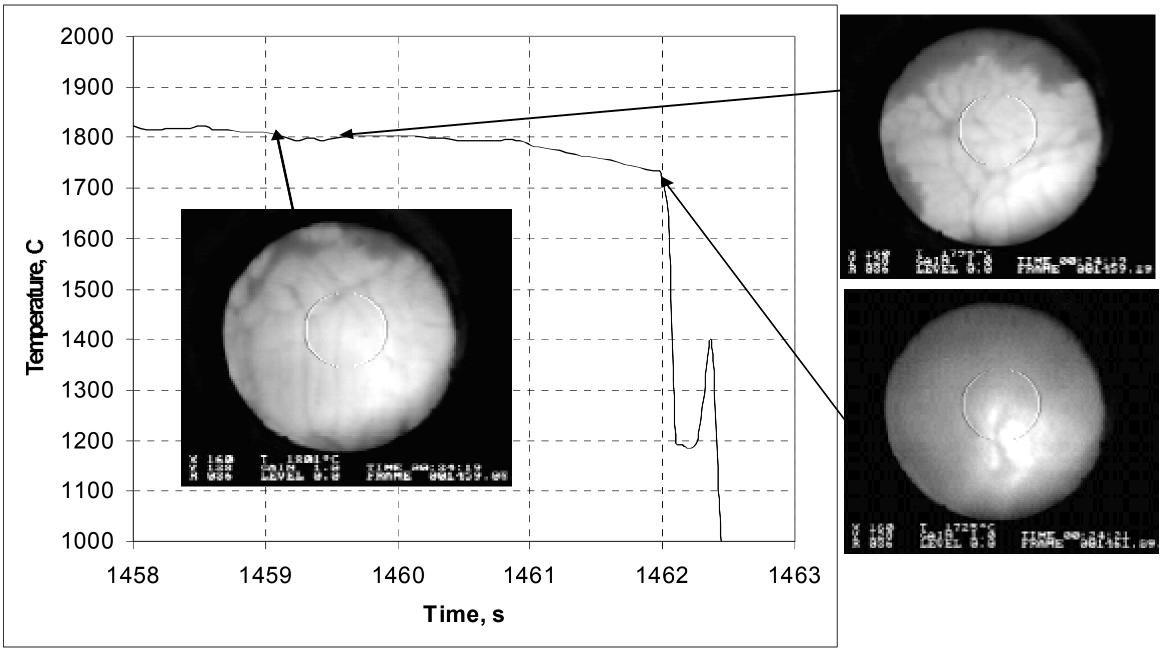

Fig. 2.33. Fragment of CORD 18 thermogram with melt surface images

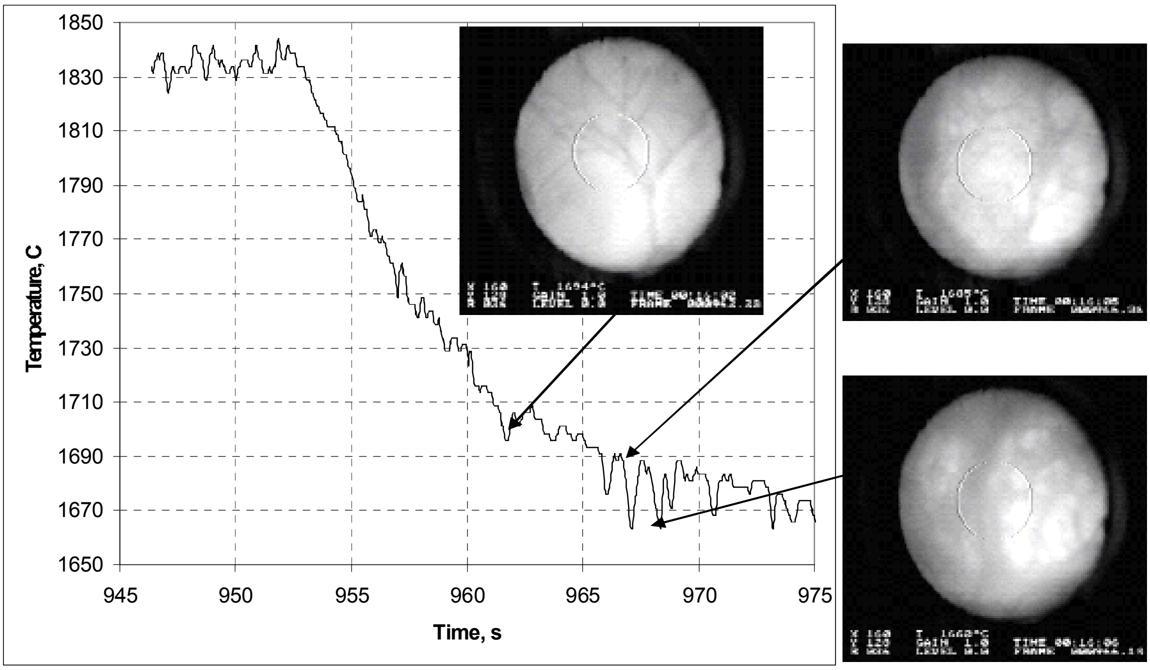

Fig. 2.34. Fragment of CORD 19 thermogram with melt surface images

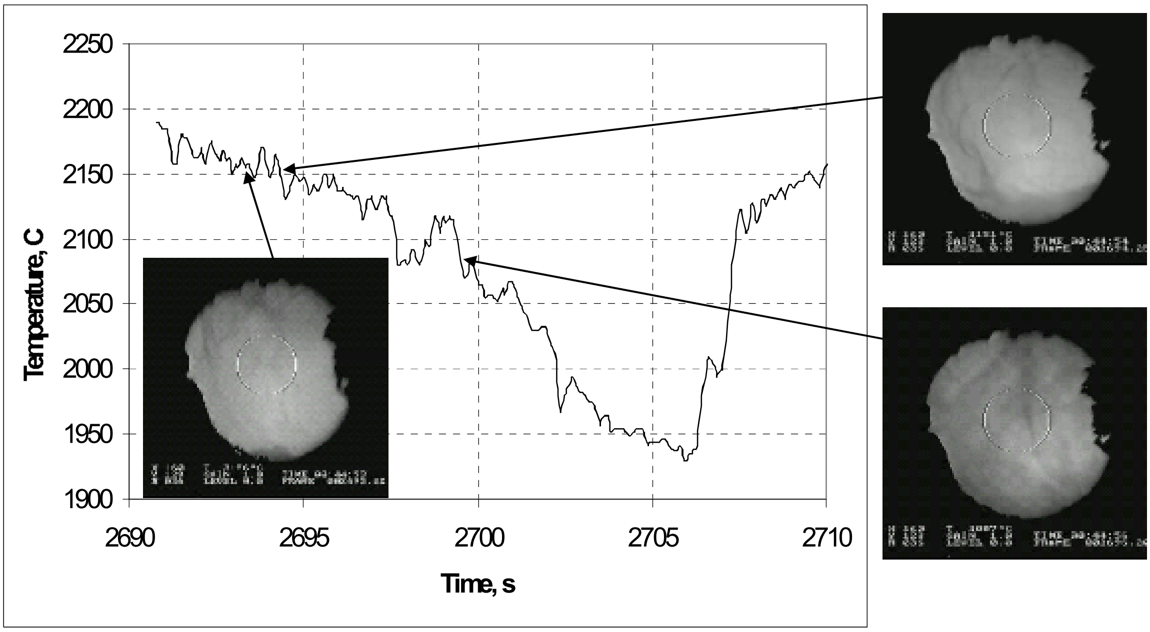

Fig. 2.35. Fragment of CORD 21 thermogram with melt surface images

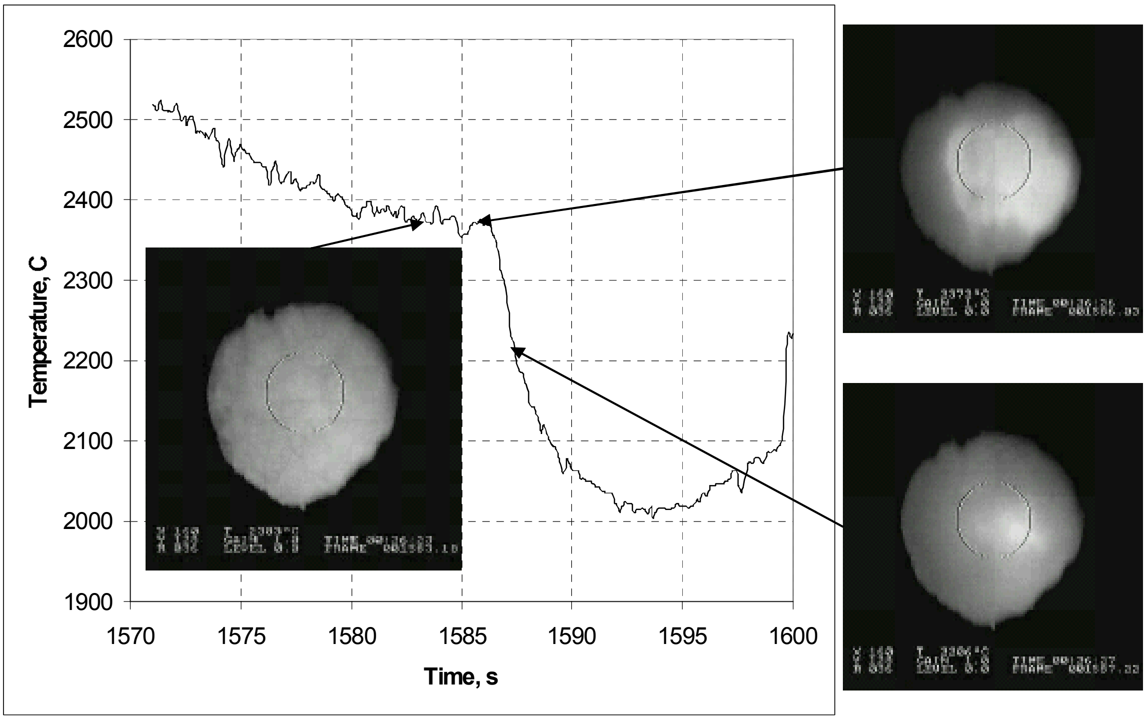

Fig. 2.36. Fragment of CORD 22 thermogram with melt surface images

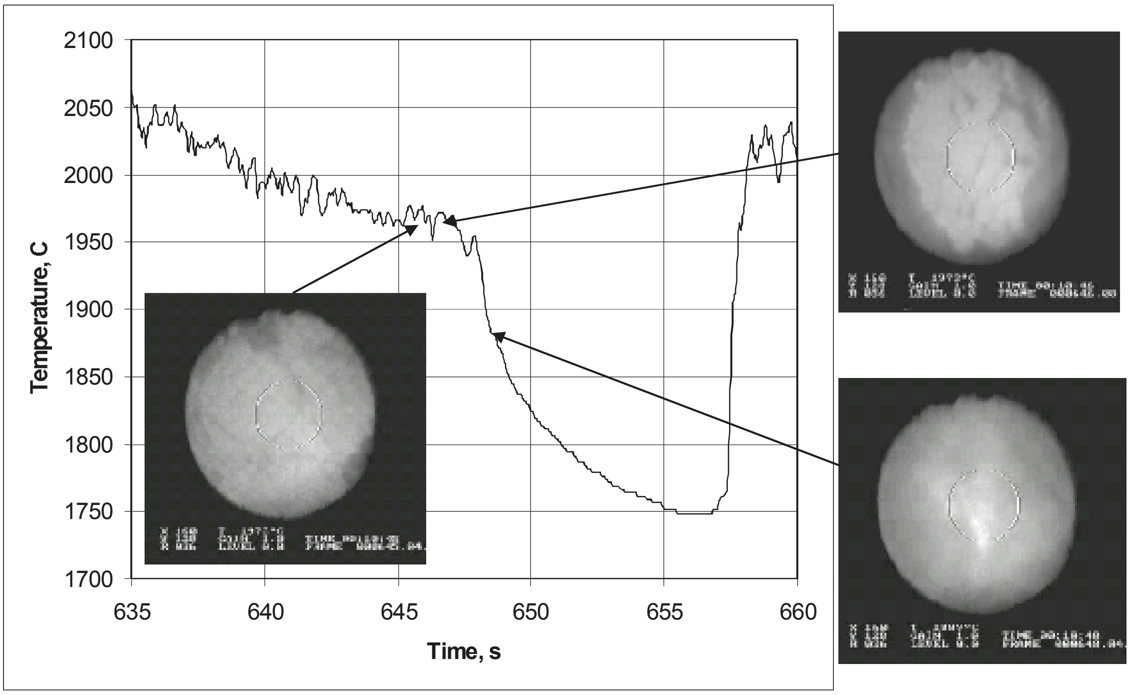

Fig. 2.37. Fragment of CORD 23 thermogram with melt surface images

Table 2.7. VPA IMCC T_{liq} measurements in the UO_2 – FeO system

CORD No.	Charge composition, mass%		Composition of melt samples in accordance with physico-chemical analysis of samples, mass%/mole%		T_{liq}, °C
	UO_2	FeO	UO_2	FeO	
8*	11.4	88.6	12-18.1/3.5-5.55	88-81.9/96.5-94.45	1330
17	40	60	32.37/11.3	67.63/88.7	1580
18	60	40	51.51/22.04	48.49/78.64	1802
19	50	50	41.77/16.03	58.23/83.97	1694
20	16.4	83.6	19.51/6.06	80.49/93.94	1370
21	80	20	76.24/46.06	23.76/53.94	2147
22	90	10	88.64/67.49	11.36/32.51	2368
23	70	30	65.79/33.85	34.21/66.15	1959

*- SEM/EDX data on melt sample composition.

3. Liquidus temperature measurements in the Galakhov microfurnace

Special specimens (chips) were prepared from CORD 17-23 melt samples for T_{liq} measurements in the Galakhov microfurnace. Their composition was determined by the EDX analysis.

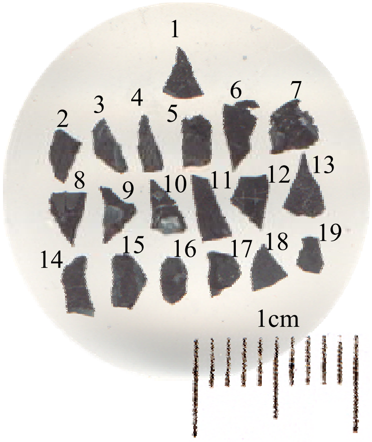

Fig. 3.1. Template with chips

CORD 18 (60 mass% UO_2 – 40 mass% FeO): **1** – sampler rod 1, **2** – sampler rod 2, **3** – sample 3 bottom, **4** – sample 3 side, **5** – sample 4 bottom, **6** – sample 4 side; **CORD 17** (40 mass% UO_2 – 60 mass% FeO): **7** - sample 1 center, **8** – sample 1 edge, **9** – sample 2 center, **10** – sample 2 edge; **CORD 19** (50 mass% UO_2 – 50 mass% FeO): **11** – sampler rod 2, **12** – sample 2 side, **13** – sample 2 center, **14** – sampler rod 3, **15** – sample 5 edge, **16** – sample 5 center; **CORD 21** (80 mass% UO_2 – 20 mass% FeO): **17** – sample 3; **CORD 23** (70 mass% UO_2 – 30 mass% FeO): **18** – sample 2 bottom, **19** – sample 2 edge

Fig. 3.1 shows a template with chips and their position. Figs. 3.2 – 3.7 present their SEM/EDX data.

CORD 18

In comparison to the initial charge the refractory component is depleted in the average composition of chips 1-6, as well as in the average composition of CORD 18 ingot center (see Fig. 3.2). The content of UO_2 in samples 1-5 varies within 39-43 mass.% (the vertical variation of UO_2 concentration in the ingot was 35-43 mass.%, which approximately corresponds to the range of sample composition variations). The microstructure of chips comprises smaller and more evenly distributed dendrites, which form UO_2-based refractory frame, which prevents the early spreading of the specimen and reduces the error in T_{liq} measurements made by the visual polythermal methods. It should be noted that chip 6 (side, taken by the spoon) is very inhomogeneous and features the highest depletion of the refractory component. High porosity of some chips should also be noted.

Two chips of sample 4, bottom (Fig. 3.1) have been studied by the VPA in the Galakhov microfurnace. The sample was chosen, because it was taken when melt temperature was close to T_{liq}.

Sample microstructure (chip 5) is quite suitable for the VPA studies.

T_{liq} measured in the microfurnace was 1520 °C for one chip and 1515 °C for another. It should be noted that their composition after the microfurnace has not been studied. The microanalysis of chips 5 and 6 enables to assume that the content of uranium oxides is within 11.67-16.26 mole % UO_2.

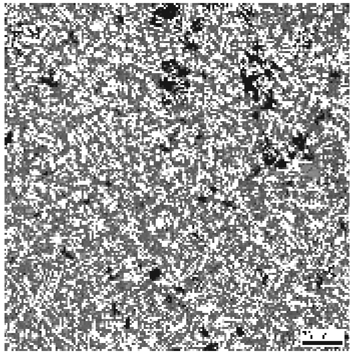

Microphotograph of chip 1

No.		UO_2	FeO
SQ	mass%	39.67	60.33
	mole%	14.89	85.11

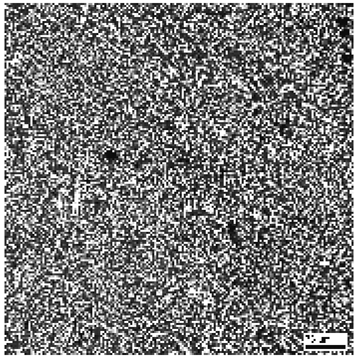

Microphotograph of chip 2

No.		UO_2	FeO
SQ	mass%	39.27	60.73
	mole%	14.68	85.32

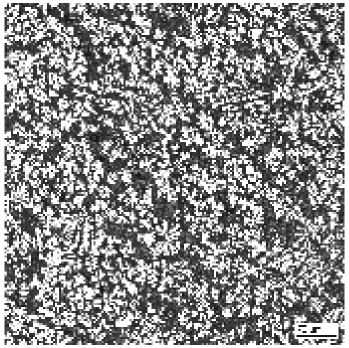

Microphotograph of chip 3

No.		UO_2	FeO
SQ	mass%	42.08	57.92
	mole%	16.2	83.8

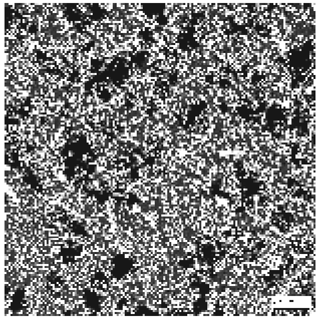

Microphotograph of chip 4

No.		UO_2	FeO
SQ	mass%	39.21	60.79
	mole%	14.65	85.35

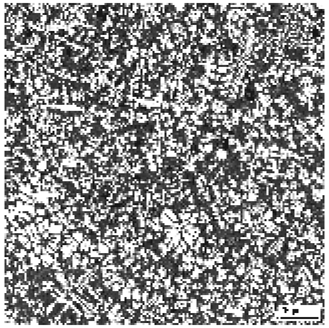

Microphotograph of chip 5

No.		UO_2	FeO
SQ	mass%	42.19	57.81
	mole%	16.26	83.74

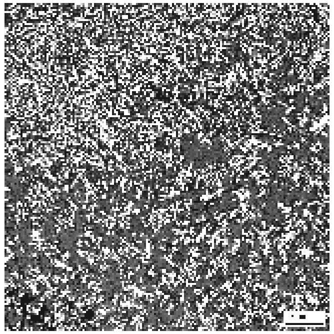

Microphotograph of chip 6

No.		UO_2	FeO
SQ	mass%	33.19	66.81
	mole%	11.67	88.33

Fig. 3.2. Microstructure and EDX analysis of chips 1-6, CORD 18

CORD 17

The average composition of chips 7-10, and of the CORD 17 ingot center demonstrates the depletion of refractory component in comparison to the initial charge (see Fig. 3.3). Composition of chip 9 is very close to eutectics. The content of UO_2 in chips 7, 8, 10 varies within 23-27 mass.% (in the ingot the concentration of UO_2 was 23 mass%). Therefore, on the average, the chips are more enriched with refractory components that the ingot. The chips are very inhomogeneous and porous. Their typical regions differ from the ingot central part by smaller and more evenly distributed dendrites.

Two chips of sample 2, center, were subjected to the VPA in the Galakhov microfurnace. T_{liq} measured in the microfurnace was 1470°C for one chip and 1456°C – for another. Sample 2 was taken when the screen was lowered and mushy zones appeared on the melt surface, for this reason the composition inhomogeneity across the sample cross-section is observed. Nevertheless the reproducibility of values measured in the microfurnace is acceptable, and the composition of studied chips can be attributed to the range of 23-27 mass % UO_2.

CORD 19

In comparison to the initial charge the refractory component is depleted in the average composition of chips 11-16 (see Fig. 3.4). The content of UO_2 in chips 11-15 varies within 27-33 mass.% (in the ingot the UO_2 concentration was ~18 mass.%, but this is a composition after a thick layer was grown in conditions of equilibrium crystallization). Chip 16 includes the region of pure FeO, so its average composition has an even higher depletion of the refractory component. All chips are rather homogeneous (except 16). Like in the previous chips the refractory phase got crystallized as small and evenly distributed dendrites. Two chips of sample 5, center, were subjected to the VPA in the Galakhov microfurnace. T_{liq} measured in the microfurnace was 1625°C for one chip and 1560°C - for another.

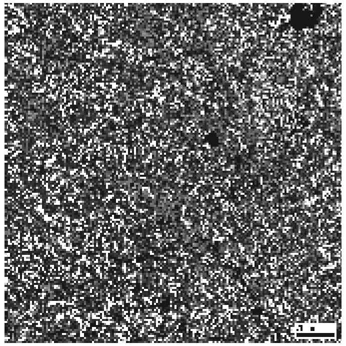

Microphotograph of chip 7

No.		UO_2	FeO
SQ	mass%	24.48	75.52
	mole%	7.94	92.06

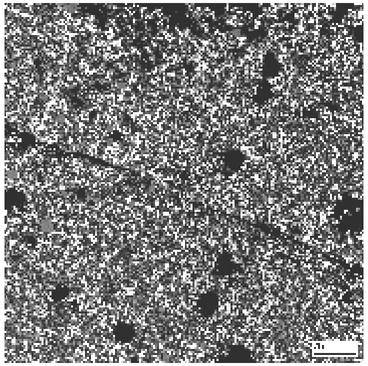

Microphotograph of chip 8

No.		UO_2	FeO
SQ	mass%	26.78	73.22
	mole%	8.87	91.13

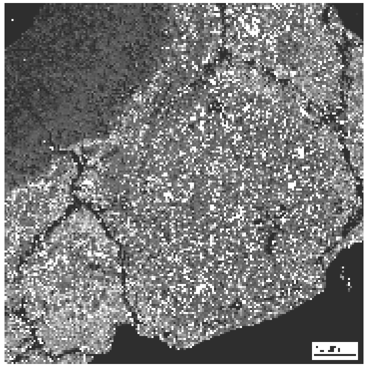

Microphotograph of chip 9

No.		UO_2	FeO
SQ	mass%	12.38	87.62
	mole%	3.62	96.38

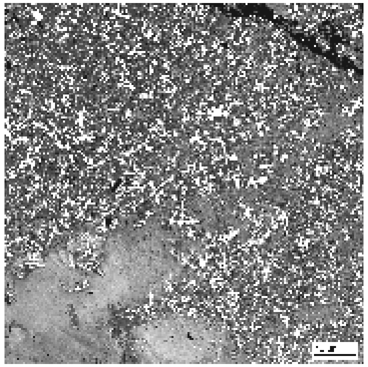

Microphotograph of chip 10

No.		UO_2	FeO
SQ	mass%	22.74	77.26
	mole%	7.26	92.74

Fig. 3.3. Microstructure and EDX analysis of chips 7-10, CORD 17

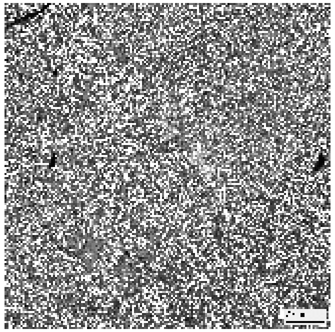

Microphotograph of chip 11

No.		UO_2	FeO
SQ	mass%	30.61	69.39
	mole%	10.51	89.49

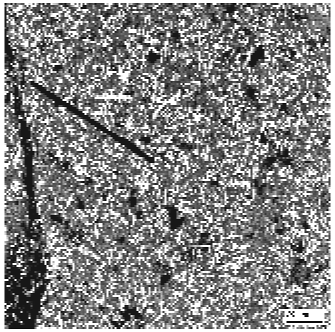

Microphotograph of chip 12

No.		UO_2	FeO
SQ	mass%	28.14	71.86
	mole%	9.44	90.56

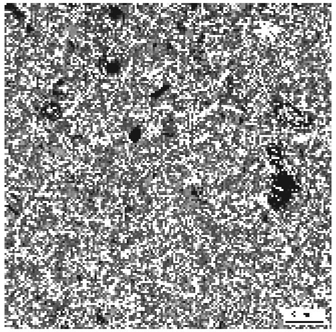

Microphotograph of chip 13

No.		UO_2	FeO
SQ	mass%	33.21	66.79
	mole%	11.68	88.32

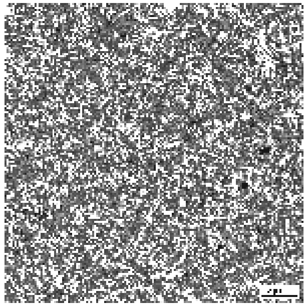

Microphotograph of chip 14

No.		UO_2	FeO
SQ	mass%	32.19	67.81
	mole%	11.22	88.78

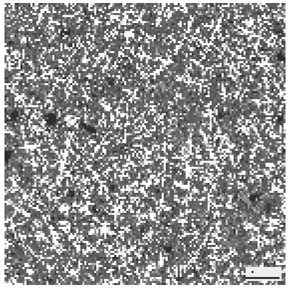

Microphotograph of chip 15

No.		UO_2	FeO
SQ	mass%	26.92	73.08
	mole%	8.93	91.07

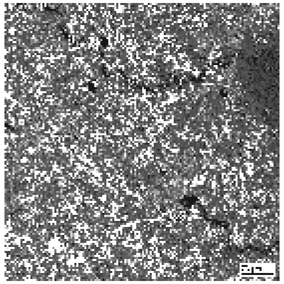

Microphotograph of chip 16

No.		UO_2	FeO
SQ	mass%	22.21	77.79
	mole%	7.06	92.94

Fig. 3.4. Microstructure and EDX analysis of chips 11-16 CORD 19

CORD 21

In comparison to the initial charge the refractory component is depleted in the average composition of chip 17 (see Fig. 3.5). The content of UO_2 in it is ~65 mass.% (in the ingot its concentration varied within 58 - 68 mass.%). The refractory phase was crystallized as small and evenly distributed dendrites.

One chip of sample 3 has been studied by the VPA in the Galakhov microfurnace. T_{liq} measured in the furnace was 2020 °C.

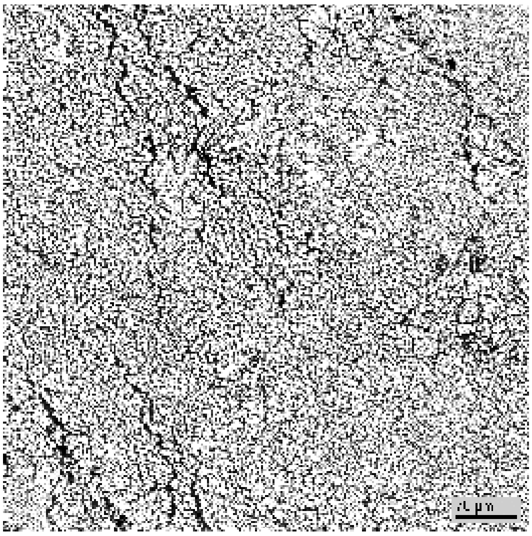

Microphotograph of chip 17

No.		UO_2	FeO
SQ	mass%	65.05	34.95
	mole%	33.12	66.88

Fig. 3.5. Microstructure and EDX analysis of chip 17 CORD 21

CORD-23

In comparison to the initial charge the refractory component is depleted in the average composition of chips 18-19 (see Fig. 3.5). The content of UO_2 in the chips varies within 53-54 mass.% (UO_2 concentration in the ingot was ~49 mass). The refractory phase got crystallized as small and evenly distributed dendrites.

A chip of sample 2, bottom, has been studied by the VPA in the Galakhov microfurnace. T_{liq} measured in the microfurnace was 1815 °C.

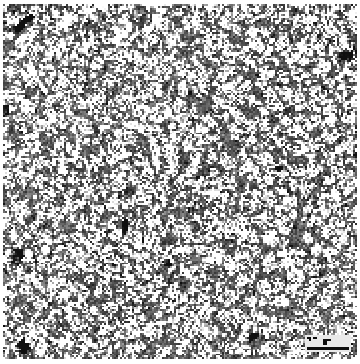

Microstructure of chip 18

No.		UO_2	FeO
SQ	mass%	52.98	47.02
	mole%	23.06	76.94

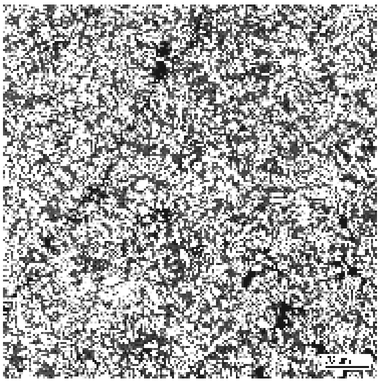

Microstructure of chip 19

No.		UO_2	FeO
SQ	mass%	54.11	45.89
	mole%	23.88	76.12

Fig. 3.5. Microstructure and EDX analysis of chips 18-19, CORD 23

Therefore, all studied specimens have demonstrated a strong composition shift towards the fusible component and an occasionally wide range of concentrations. In order to reduce the error of correlating T_{liq} with a certain concentration a decision was taken to determine the UO_2-FeO sample composition after the Galakhov microfurnace.

CORD 21

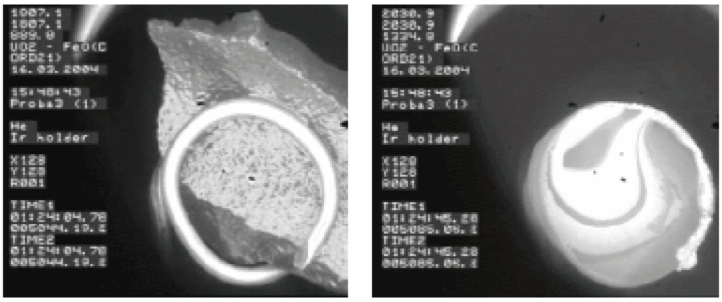

1 2

Sample 3 (first melting) during the test (iridium holder):
1 – melting start (T=1807.1 °C); 2 – complete melting of the specimen (T=2030.9 °C)

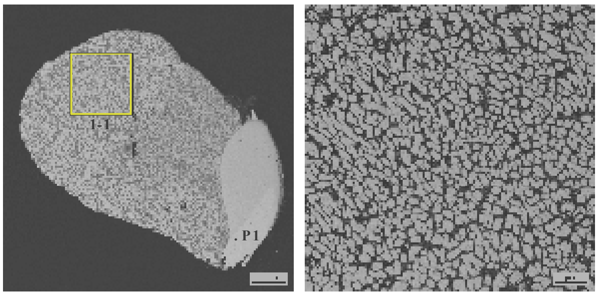

1 1-1(SQ1)

Microphotograph of a chip from sample 3 (first melting)

No.		UO_2	FeO
SQ1	mass%	70.55	29.45
	mole%	38.48	61.52
P1		100% Ir	

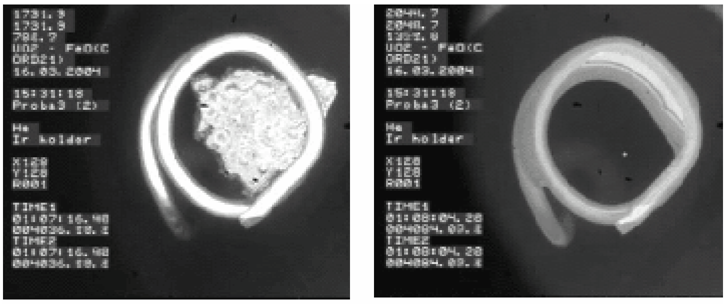

1 2

Sample 3 (second melting) during the test (iridium holder):
1 – melting start (T=1731.9 °C); 2 – complete melting of the specimen (T=2048.7 °C)

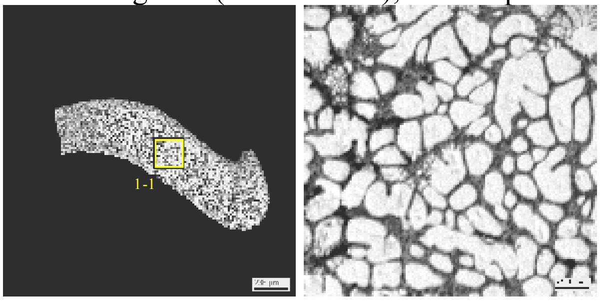

1 1-1(SQ1)

Microphotograph of a chip from sample 3 (second melting)

No.		UO_2	FeO
SQ1	mass%	74.64	25.36
	mole%	43.47	56.53

Fig. 3.6. Sample during the test, microstructure and EDX analysis of the sample after melting in the Galakhov microfurnace

The microphotographs (Fig.3.6) show the fragments of molten specimens (chips). A considerable difference of chips prepared from the same sample should be noted. The microphotograph of a chip from specimen 3 (first melting) shows the iridium holder (Point R1) and molten specimen (Area SQ1). T_{liq} of this specimen measured by the VPA in the Galakhov microfurnace is 2031 °C. The interaction between specimen and iridium holder was noticeable.

The microphotograph of a chip from specimen 3 (second melting) shows the fragment of a molten specimen, T_{liq} of this specimen measured by the VPA in the Galakhov microfinance was 2049 °C.

CORD 23

Microphotographs of Fig. 3.7 show the fragments of molten specimens. T_{liq} of the specimen measured by the VPA in the Galakhov microfurnace was 1733 °C in the first melting, and 1865 °C - in the second.

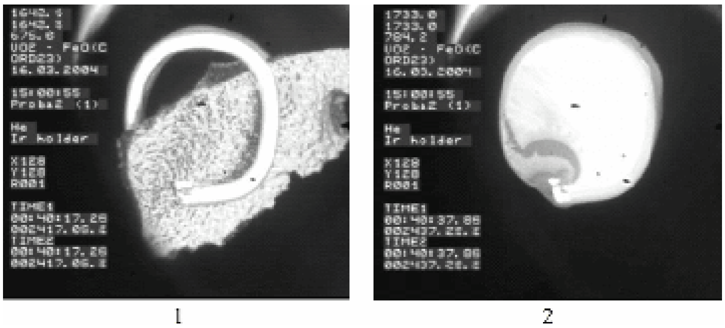

Sample 2, bottom (first melting) during the test (iridium holder):
1 – melting start (T=1642.3 °C); 2 – complete melting of the specimen (T=1733.0 °C)

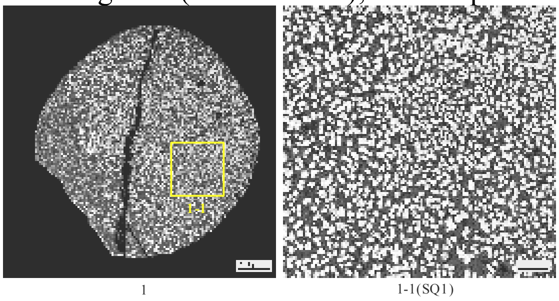

No.		UO_2	FeO
SQ1	mass%	53.7	46.3
	mole%	23.25	76.75

Microphotograph of a chip from specimen 2, bottom (first melting)

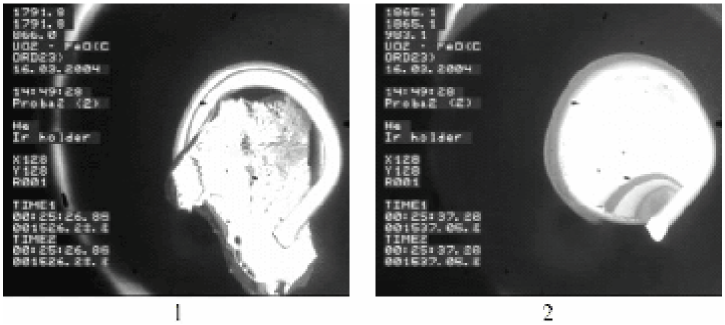

Sample 2, bottom (second melting) during the test (iridium holder):
1 – melting start (T=1791.8 °C); 2 – complete melting of the sample (T=1865.1 °C)

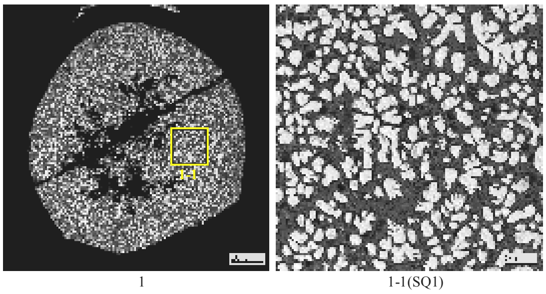

No.		UO_2	FeO
SQ1	mass%	52.94	47.06
	mole%	22.71	77.29

Microphotograph of a chip from specimen 2, bottom (second melting)

Fig. 3.7. Microstructure and EDX analysis of the sample after melting in the Galakhov microfurnace

4. Differential thermal analysis (DTA)

The DTA of samples from CORD 22 and CORD 17 was performed on the SETSYS Evolution-2400 analyzer in order to study T_{sol} (which is the eutectics temperature in the binary system). The SETSOFT 2000 software was used for data processing.

All samples have been analyzed in the same conditions:

Mass of samples was ≈ 10-15 mg, the measurement section was sparged with helium, its flow rate was 4 ml/min, the heating rate was 5 °C/min, thermocouples of B type were used - (Pt/ Pt/Rh – 30/6). The device underwent a pre-measurement calibration against the melting points of extra-pure metals.

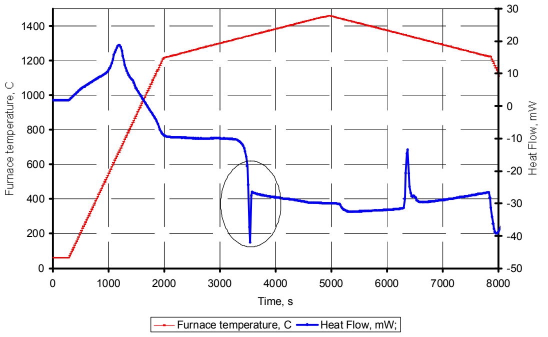

Fig. 4.1. Thermogram of sample CORD 22

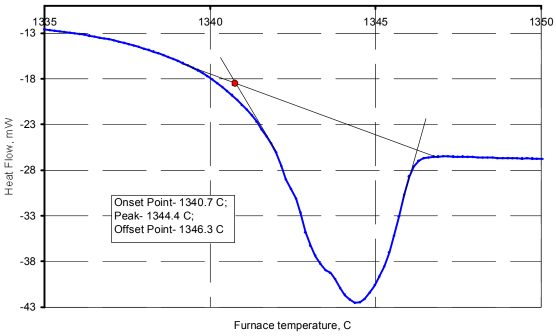

Fig. 4.2. Thermogram of sample CORD 22 – enlarged fragment (during hearing)

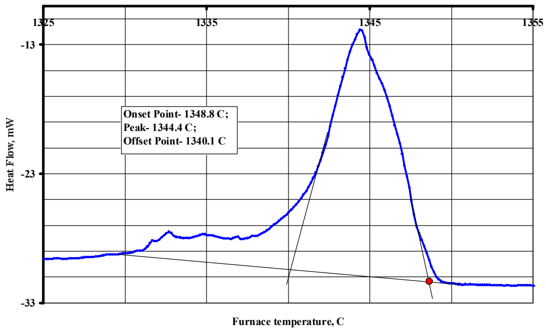

Fig. 4.3. Thermogram of sample CORD 22 – enlarged fragment (during cooling)

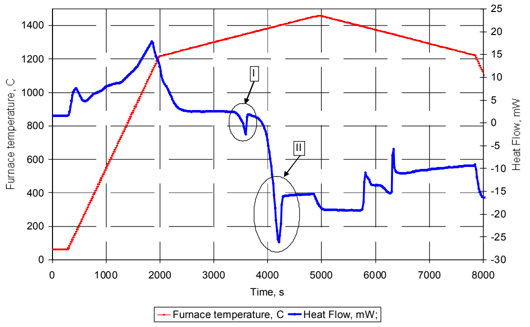

Fig. 4.4. Thermogram of sample CORD 17

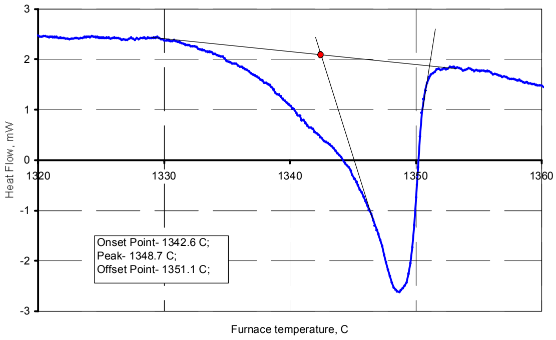

Fig. 4.5. Fragment 1, thermogram of CORD 17 sample (heating, solidus)

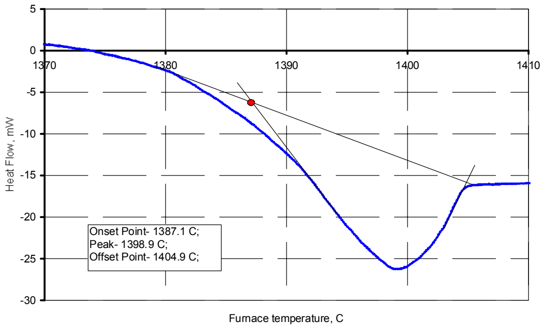

Fig. 4.6. Fragment 2, thermogram of CORD 17 sample (heating, liquidus)

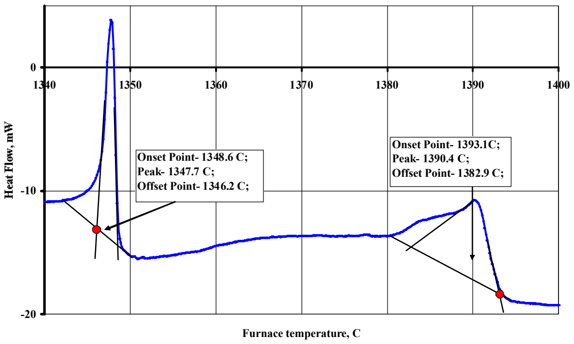

Fig. 4.7. Fragment 2, thermogram of CORD 17 sample (cooling)

Figs. 4.1-4.4 show the presence of distinct peaks indicating endothermic effects within 1340 - 1346 °C temperature interval of CORD 22 and 1342 - 1349 °C for CORD 17. The baseline “linear from first to last point” was chosen for determining the temperature corresponding to the peak start, after that tangent lines were drawn to the peak sides. The crossing point of tangent and base lines indicated 1340.7 and 1342.6 °C, respectively.

Consequently, T_{sol} (eutectics temperature) of the UO_2 –FeO system is 1342 °C. The DTA of CORD 17 sample also determined T_{liq} of an ingot sample. The composition corresponding to this temperature has not been determined due to the small quantity of studied material.

5. Discussion of results

High chemical activity of melts in the UO_2–FeO system and unavailability of crucibles for containing such melts make the T_{liq} measurements by classical methods (VPA, DTA, etc.) hardly feasible. The required studies became possible after the development and application of the VPA IMCC; one of its advantages is the absence of melt interaction with crucible materials. Studies in the Galakhov microfurnace basically confirm the VPA IMCC data (within the composition and temperature measurement error) – Table 5.1.

Table 5.1. Comparison of data produced by different methods

Experiment/method	**FeO concentration**		**Concentration error, mass. %**	**T_{liq}, °C**	**T_{sol}, °C**
	mass %	**mol %**			
CORD17/VPA IMCC	67.63	88.7	± 3.4	1580	-
CORD18/Galaknov	57.81-66.81	83.74-88.33	± 2.9 - ±3.3	1515-1520	
CORD19/VPA IMCC	58.23	83.97	± 2.9	1694	
CORD20/VPA IMCC	80.49	93.94	± 4.0	1370	
CORD21/VPA IMCC	23.76	53.94	± 1.2	2147	
CORD22/VPA IMCC	11.36	32.51	± 0.6	2368	
CORD17/Galakhov	73.22-87.62	91.13-96.38	±3.7 - ±4.4	1456-1470	
CORD19/ Galakhov	66.79-77.79	88.32-92.94	±3.3 - ±3.9	1560-1625	
CORD23/VPA IMCC	34.21	66.15	± 1.7	1959	
CORD21/ Galakhov	34.95	66.88	± 1.7	2020	
	29.45	61.52	± 1.5	2020	
	25.36	56.53	± 1.3	2050	
CORD18/VPA IMCC	48.49	78.64	± 2.4	1802	
CORD23/ Galakhov	45.89-47.02	76.12-76.94	±2.3 - ±2.4	1815	
	46.3	76.75	± 2.3	1730-1740	
CORD17/ DTA	-		-	-	1342.6
CORD22/ DTA					1340.7

During the liquidus temperature measurements by the VPA IMCC the top limit of error is less than +50°C, bottom limit – 1% from the determined value.

The error of T_{liq} determination by the Galakhov method is ±25 °C, and that of T_{sol} determination by DTA is ±5 °C. For the studied compositions the crystallization peculiarity is observed as a noticeable gradient of UO_2 concentration, which is found both in the sampler rod and spoon samples. Therefore, the physico-chemical data of average samples are different from the EDX data of the specimens taken from same samples, but representing 2 - 5% of the total sample mass.

When comparing the Galakhov microfurnace measurements we should mention that the data for one CORD 23 sample had a 75 °C difference from others. This can be explained by a strong inhomogeneity of composition in a single specimen (chip). In further investigations each Galakhov furnace studies should be followed by the EDX analysis for the identification of specimen composition.

After the SEM/EDX analysis of the CORD 8 ingot the charge composition for CORD 20, in which the eutectics position was specified, was determined.

In accordance with the experimental data the eutectics zone composition corresponds to the iron oxide content of 86.3-86.6 mass % (Fig. 2.23, segments SQ1 and SQ2). The difference between these and CIT data can be explained by a higher equilibrium in the melt crystallized during its extraction at 5-10 mm/h, and by a larger volume occupied by the eutectics core, which enabled to average an extensive area during the SEM/EDX analysis. The temperature of eutectics point determined in the current study is practically the same as in the CIT project.

The SEM/EDX analysis of first ingots has shown that crystals of solid solutions are rather small; the probe, which was scanning their composition, also covered neighboring regions. This has resulted in the distortion of data on the solid solution composition. In order to grow large solid solution crystals staying in equilibrium with the melt, the extraction of ingot in CORD 19 lasted two hours. The ingot analysis has shown (Fig. 2.21), that its periphery region was nearly a monophase UO_2 layer with FeO dissolved in it. Note that when a part of this layer gets into the subsolidus region, it decays into uranium oxide and iron oxide.

This is the phenomenon, which is probably responsible for a failure in measuring the solid solution composition in the conventional conditions of the melt crystallization, i.e. without the slow extraction. After the ingot was extracted the heating was disconnected for a restricted period of time to ensure a high cooling rate for the layer grown by extraction under subsolidus temperatures. In this way in CORD 19 the composition of solid solution was fixed before its decomposition. The composition of this solution (mass/mol% 94.82/83.26 UO_2 –5.08/16.74 FeO) is practically final, because the melt composition, which is in equilibrium with it, is close to the eutectics.

An extensive amount of SEM/EDX studies of axial ingot sections has been performed. It provides the information about the refractory system crystallization pattern and its behavior in the subsolidus region. The features of ingot micro- and macro-structure testify to the absence of miscibility gap in the studied system. A strong shift of the melt composition as compared to the initial charge has been revealed, which is explained by the crystallization of the refractory component on the cooled surfaces of the pool. The metallic iron inclusions have been found in all ingots, which confirms the system stoichiometry, but complicates a further analysis of samples by the Galakhov and DTA methods.

During the DTA examination of samples having eutectics composition, which was performed in tungsten crucibles, the produced melt wetted tungsten and crept up the crucible walls, which resulted in the distortion of thermogram and excluded its interpretation. T_{liq} of other compositions has not been measured for the same reason. But this method ensured a high accuracy of T_{sol} (eutectics temperature) measurements. In accordance with DTA it was 1342±5 °C.

Conclusions

1. The eutectics composition and temperature in the system have been determined; they correspond to the iron oxide concentration 86.4±2.5 mass% and 1342±5 °C.
2. The determined maximum value of solubility limit of FeO in cubic UO_2 is 5±1 mass% at eutectic temperature.
3. The UO_2 – FeO liquidus line has been constructed using the experimental data.
4. These results can be used for optimization of databases on phase diagrams.

Fig. 5.1 presents the fusibility diagram of the FeO - UO_2 system, which was constructed on the basis of experimental data provided by different methods.

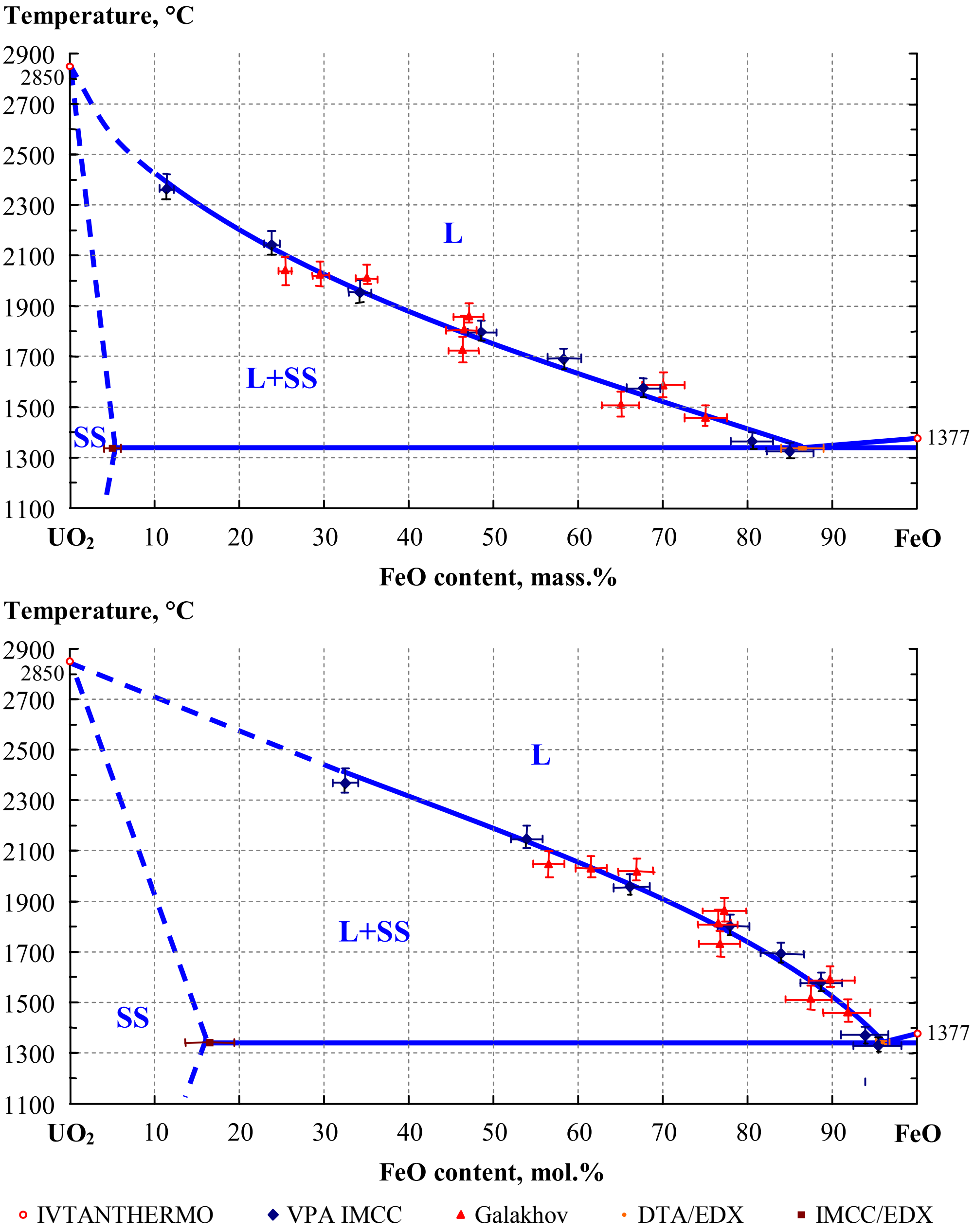

Fig. 5.1. Phase diagram of the UO_2-FeO system

References

1. G.V. Belov. Thermodynamic modeling: methods, algorithms, programs. - M.: Nauchny Mir, 2002.-184 p. (In Russian)
2. http://thermodata.online.fr/
3. V.V. Gusarov, S.V. Sobakin, Yu.P. Udalov. Information and analysis system on phase diagrams of multi-component oxidic systems // Proceedings of the meeting "Computer methods in the control of electrotechnological regimes of the ore-smelting furnaces ELECTROTERMIA-98", June 2-3, 1998, St. Petersburg (In Russian)
4. http://www.npl.co.uk/
5. MTDATA - The NPL databank for metallurgical thermochemistry Davies R H, Dinsdale A T, Hodson S M, Gisby J A, Pugh N J, Barry T I, Chart T G, *Proc. Conf. "User Aspects of Phase Diagrams"*, 25-27 June 1990, Petten, Institute of Metals.
6. O.V. Mazurin, V.V. Gusarov. Future of information technologies in material studies // Physics and chemistry of glass. V.28. N1. 2002 p.74-85. (In Russian)
7. Belov G.V., Iorish V.S., Yungman V.S. IVTANTHERMO for Windows - database on thermodynamic properties and related software. // CALPHAD.- 1999. V.23, No. 2. - P. 173-180.
8. http://www.msm.cam.ac.uk/, www.factsage.com
9. NUCLEAR04 Database, INPG/CNRS/THERMODATA, Test version, 2004
10. http://www.ceramics.nist.gov/, NIST Standard Reference Database #30, Version April 2003
11. Epstein L.F., Howland W.H. J. Amer. Ceram. Soc., 36, No.10, 334, 1953.
12. New Experiments on the Interaction of ZrO_2 Material with Corium Melts and Phase Diagram Points in UO_2-Based Systems. CIT Project Report, Corium Interactions and Thermochemistry, In-Vessel Cluster, INV - CIT(99)-P037, December 1999.
13. N.M. Voronov et al. High-temperature chemistry of uranium oxides and their compounds. M., Atomizdat, 1971. (In Russian).
14. L.M. Viting. High–temperature solutions and melts. M. MGU Publishing House. 1991. (In Russian).
15. ENTHALPY [Generation of data for phase diagrams of multi-component oxidic mixtures, based on prototypic molten corium. ENTHALPY Project report: "European Nuclear Thermodynamic Database validated and applicable in Severe Accidents" First stage, LSK, May 2001.
16. Generation of data for phase diagrams of multi-component oxidic mixtures, based on prototypic molten corium. ENTHALPY Project report: "European Nuclear Thermodynamic Database validated and applicable in Severe Accidents" Second stage, LSK, March 2002.
17. Generation of data for phase diagrams of multi-component oxidic mixtures, based on prototypic molten corium. ENTHALPY Project report: "European Nuclear Thermodynamic Database validated and applicable in Severe Accidents" Third stage, LSK, December 2002.
18. Liquidus and solidus temperature measurements in the subsystem UO_2-ZrO_2-(SiO_2-FeO_x-CaO-Al_2O_3-Cr_2O_3). ENTHALPY Project Report, European Nuclear Thermodynamic Database, Tasks 2.2.3, 2.4 and 2.5.1, SAM–ENTHA(03)–D011, June 2003.

19. S.V. Stepanova., Yu. Tsivinsky, L.M. Zatulavsky, V.A. Kopylov, D.Ja. Kravetsky. Determination of the axial temperature gradient and subcooling at the crystallization front during the production of sapphire by the Stepanov methodology // Crystallography, 1982, V.27, issue 3. p. 578-583. (In Russian)
20. M.V. Pikunov. Melting of metals, crystallization of alloys, freezing of ingots. M. MISIS. 1997. (In Russian).
21. New miscibility gap for ex-vessel corium oxide compositions"-Y. Petrov, Y. Udalov, K. Jurek, P. Sazavsky, M. Kiselova, P. Selucky , C. Journeau, P. Piluso\\ ICAPP' 04 , Pittsburgh, PA USA, June 13-17, 2004. Paper 4077
22. F.Ja. Galakhov. High-temperature furnace for studying heterogeneous equilibria in the refractory oxidic systems.-In.: Modern methods of studying silicates and construction materials. M.,1961 p. 178-182. (In Russian).
23. A.A. Fedorov. New methods for analyzing metallic powders and slags. "Metallurghia" Publishing House, 1972. (In Russian).
24. V.K. Markov et al. Uranium. Methods for its detection. M., Atomizdat, 1964. (In Russian).
25. E. Sendel. Colorimetry methods for the determination of metal traces. M.., Mir ,1964(In Russian)
26. Harvey, Smnart, Amis, Anal. Chem., 27, 26 (1955).
27. T.M. Florence- Analytical methods in the nuclear fuel cycle/ Vienna: JAEA, 1972.
28. Methods for determining the O/U ratio in the substoichiometric uranium dioxide. Radiochemistry, V.36, issue 3, 1994 (In Russian).
29. D.I. Riabchikov, M.M. Seniavin. Analytical chemistry of uranium. M. Publishing House of the USSR Academy of Sciences. 1962 (In Russian)
30. V.F. Lukianov, S.B. Savvin, I.V. Nikolskaya. Photometric detection of uranium in micro-quantities with arsenazo reagent III. JACh., V. XV, issue 3. 1960. (In Russian)
31. N.F. Losev. Quantitative XRF. M.: Nauka, 1969. (In Russian)